RESPONSES TO REVIEWERS

Ms. Ref. No.: Atmos. Meas. Tech. Discuss., doi:10.5194/amt-2019-252.

Title: Discrete-wavelength DOAS NO_2 slant column retrievals from OMI and TROPOMI

Response to Anonymous Referee #1

The manuscript "Discrete-wavelength DOAS NO_2 slant column retrievals from OMI and TROPOMI" describes a NO_2 retrieval algorithm based on the DOAS method with discrete spectral channels. The idea of discrete channels has been applied for ozone retrieval, and its potential for NO_2 retrieval is shown in this manuscript, addressing the advantage of simpler instrumental design. The retrieval is implemented for OMI and TROPOMI data with good agreement with respect to reference products (5% difference for OMI and 11% difference for TROPOMI). Critical issues like the selection of discrete channels, uncertainties, and limitations are discussed. The topic of the manuscript is within the scope of AMT.

My major concern with this manuscript is the verification or validation. In principal the overall quality of a retrieval needs to be evaluated by comparisons with independent satellite retrievals or by comparisons with correlative ground-based measurements (e.g., direct sun measurements from Pandora). Since the authors have shown only specific days as examples for comparisons with reference datasets, the retrieval quality can hardly be analysed without a longer time series reprocess of OMI and TROPOMI slant column data and additional comparisons, which are particularly important for discrete-wavelength DOAS (with no wavelength calibration). Therefore I recommend that the authors include more verification or validation results to check for possible systematic bias or temporal drift of differences.

Thank you for your comment. We agree that further validation would be needed if the aim was to establish a new method to retrieve NO_2. However, the work presented in this paper is intended only as a proof of concept rather than a comprehensive validation of a new product. Thus, for this purpose the reference OMI and TROPOMI level 2 products are considered as the "truth" and our retrieval results validated against them. We selected four days from different seasons to get a range of solar angles and prevailing atmospheric conditions, and we used global data to factor in a wide range of atmospheric scenarios and spatial differences. The differences between our retrieval and the reference products are consistent across all the data with the exception of some spatial differences, which we have already discussed in the text. It is expected that the main factor affecting a time series would be noise from the degradation of the instrument, which would manifest in the form of higher scatter in the DW-DOAS retrieval. Therefore, the authors feel that further validation is beyond the scope of this paper, but are currently working on more comprehensive sensitivity analyses and validation which will be the focus of the next paper. We have clarified in the text that the focus of the paper is only to perform a proof of concept.

Another general request is that please follow the standard use of mathematics notation in the literature. For instance, an upright bold symbol needs to be used in the equation and text to make it clear where vectors and matrices are discussed, and also a matrix is usually written enclosed in square brackets.

We have now corrected the mathematical expressions.

The absolute differences are plotted in the appendix, but the analysis in the manuscript only focuses on the relative differences. For instance, "the largest differences around the equator" is actually only valid for the relative difference figure 5 (due to the small absolute values). Please add more discussions of the absolute differences.

Thanks for spotting this. We have added more discussion of the absolute differences.

Specific comments

P2 L21 Generally the observation is separated into in situ measurements and remote sensing measurements, and the remote sensing technique can be further separated into space-based and ground-based category.

Very good point. We have added the ground-based remote sensing technique and included a couple of examples provided by Anonymous Referee #2.

P4 L3 What has been decreased by 0.5%? Do you mean 0.5% of the degradation?

This refers to the performance of OMI's visible channel, which has had a radiometric degradation of ~0.5%. We have now modified the statement to make it clearer.

P4 L19 Please give the full name of SNR.

We added the full name and put the acronym in brackets, i.e. signal-to-noise ratio (SNR).

P7 L5 x shall be a column vector.

Corrected.

P8 Table 1. Should the fitting window for DW-DOAS be 425-450 nm (425-450 nm appears also in Table 2)?

Thanks for spotting this inconsistency. Yes, even though the first wavelength used in DW-DOAS sits around 430 nm, the fitting window should read '425-450 nm'. This range was selected from the literature. The concept of "fitting window" does not apply in the same way as it does in hyperspectral

DOAS retrievals, since we are not using continuous spectra. It should rather be interpreted as a spectral range from where we select our ten discrete wavelengths. We have modified Table 1 and added a line discussing the different interpretation of the fitting window in the context of DW-DOAS.

P9 L26 Why are the negative biases related to the differences in the fitting window? Theoretically the differences in the fitting window shall affect only the scatter of the NO_2 columns (i.e. noise) but not the fitted value of NO_2 column.

Wider fitting windows have traditionally been used to achieve higher signal-to-noise ratios. However, when such windows are used there is a higher chance of introducing other spectral signatures that are not accounted for in the retrieval, resulting in systematic biases (Richter et al., 2011). Evidence of this effect specific to the two windows used in this work can be found in Figure 11 of van Geffen et al. (2015), where changing the fitting window from 405 – 465 nm to 425 – 450 nm causes the fitted SCD to change by up to +0.5E15 molecules cm^{-2}. We have added a line explaining this.

P10 L17 What is the reason of more outliers for lower cloud radiance fractions for OMI and the opposite for TROPOMI? Also what is the impact of cloud height on these plots? Generally the retrieved column should depend strongly on the bulk height of clouds. High clouds mask the signal from surface NO_2 while for low clouds the satellite observations remain sensitive to the NO_2 in the free troposphere.

We agree with this assessment, and have amended the manuscript accordingly. However, we do not believe that a fair comparison can be made between the two results. For instance, it must be noted that the OMI and TROPOMI observations are over a decade apart and so will be subject to very different cloud structures. Additionally, TROPOMI has a smaller pixel size and so will experience very different cloud radiance fractions to OMI (see Krijger et al, 2007). Finally, there may also be inherent differences between the cloud top heights observed by both instruments based on the different retrieval algorithms they employ; OMI retrieves this parameter using the O_2-O_2 absorption feature at 477 nm (Veefkind et al, 2016), while TROPOMI makes use of the O_2-A band in its operational retrieval (Loyola et al, 2018). In addition, the QA4ECV product for OMI includes an intensity offset correction, which is not included in the TROPOMI product, and that may explain some of the differences over the ocean (Oldeman, 2018).
In addition, we have updated Figure 8 as there was a plotting error whereby the x and y axes were swapped.

P12 L14 The spatial patterns might be related to the intensity offset correction. The intensity offset correction included in the TROPOMI reference algorithm compensates spectral structures of liquid water, vibrational Raman scattering on H_2O molecules, and possible instrumental issue, leading to a difference over the cloud-free tropical ocean. Please refer to the QA4ECV report for more discussion. In addition, the pattern can also be seen a bit from the OMI absolute difference plot, but it is

overwhelmed in the relative difference plot. Therefore more analysis about the absolute results has been required (see the major comments).

Thanks for the suggestion. The TROPOMI product doesn't include an intensity offset correction. However, the OMI QA4ECV product does and we agree that it could well explain some of the spatial differences. We have now added more discussion about this and the absolute results.

Response to Anonymous Referee #2

This manuscript presents a simplified NO_2 slant column retrieval approach, which makes use of a limited number of wavelengths in an otherwise classical DOAS retrieval framework. The approach is tested on sample data from the OMI and TROPOMI sensors, and results are discussed in terms of their consistency with standard retrievals. It is concluded that retrievals based on strongly sub-sampled spectra (only 10 wavelengths are used) still provide good NO_2 slant columns. Although this result is not surprising as such (given the high quality of the original measurements), the small reduction of the noise on the retrieved slant columns is in my view a bit unexpected and worth pointing out (and possibly explain). So we come with the conclusion that retrieving NO_2 columns from 10 spectral points is feasible.

There are however a number of drawbacks and limitations in doing so, and one may wonder whether the potential advantages of reducing the spectral information would actually compensate these drawbacks. The fundamental motivation behind the study relies on the postulate that reducing the spectral information would allow to simplify instrumental design (of future satellite missions) leading to potentially improved spatial resolution at low cost. Statements along these lines are given at several places in the manuscript, but without any further elaboration, e.g. what kind of instrumental solution could be adopted? More importantly, key requirements on spectral accuracy and stability that would need to be considered for such a design are not mentioned at all. It is basically assumed that spectral performances equivalent to those of OMI and TROPOMI can "easily" be obtained with low-cost imaging systems suitable for integration on small satellites. To my opinion, the lack of such a discussion significantly limits the relevance and impact of the study. I therefore recommend publication only if these questions are better addressed in a major revision of the manuscript.

Thank you for your comment. Our intention was to demonstrate that the concept of retrieving NO_2 using only 10 discrete wavelengths is feasible and that accuracy comparable to existing level 2 NO_2 products can theoretically be achieved. We absolutely agree that in practice the concept is more complex and there are implementation challenges that must be overcome, e.g. co-registration of the spectral bands. While the study was deliberately discussed in generic terms, i.e. independent of any specific instrument solution, we acknowledge that the manuscript would benefit from more discussion about implementation challenges and potential instrument solutions. We have now added such discussion in paragraph 3 of the conclusions. Regarding the key requirements on spectral stability and accuracy, those are the focus of the next study, which we are currently working on to derive such requirements from sensitivity analyses.

Specific comments

Pg. 2, line 25: not all sources of tropospheric NO_2 are anthropogenic in nature. Please complete.

We did not intend to suggest that all sources of tropospheric NO_2 are anthropogenic, but rather that anthropogenic emissions are the main contributor. We have clarified this in the text and completed the statement with examples of natural sources of tropospheric NO_2.

Pg. 2, line 43: in addition to in-situ and satellite techniques, also ground-based remote sensing constitute a key component of the atmospheric composition monitoring system. This includes e.g. the Network for the Detection of Atmospheric Composition Change (NDACC) or the emerging Pandonia/PGN network.

Thanks for pointing this out, also highlighted by Anonymous Referee #1. We have now mentioned the ground-based remote sensing technique and given the suggested examples.

Pg. 2, line 48: current satellite instruments are limited in resolution, but TROPOMI is already doing much better than OMI. This should already be mentioned here, with a mention that ultimate resolutions in the range of 1x1 km^2 are needed to allow for individual source identification.

Thanks for your comment. We now give the example of TROPOMI instead of OMI, and mention the spatial resolution requirement for point source identification.

Pg. 2, line 56: The current resolution of TROPOMI at true nadir is 3.5 x 5.5 km^2.

We have now clarified that the stated resolution is at *true* nadir.

Pg. 3, line 71: the Brewer instrument is cited here as an example for a NO_2 measuring system based on a few wavelengths; however it is well-known that Brewer NO_2 measurements are dramatically lacking sensitivity. This was actually at the origin of the development of the Pandora instrument, which uses simple (low-cost) grating spectrometers to (strongly) improve the quality of NO_2 column measurements.

Thanks for pointing this out. We have added the lack of sensitivity as another drawback of the Brewer spectrometer.

Pg. 3, line 75: what are the "specific viewing geometries" that prevent usage of the NO_2 camera for space applications? Please clarify.

The algorithm used in the AOTF-based NO_2 camera as described in Dekemper et al. (2016) relies on clear-sky pixels being present in the scene for background subtraction. In addition, the sequential sampling of wavelengths poses a limitation to the speed at which they can be registered, making the retrieval challenging for non-static scenes. These drawbacks make the NO_2 camera unsuitable for nadir-viewing space applications. We have clarified this in the text.

Pg. 4, line 116: describe in short the interpolation method used by Bucsela, and its added value for this study

The method used by Bucsela et al. (2006) calculates the interpolated spectrum using the high-resolution solar reference spectrum as follows:

$$F(\lambda + d\lambda) = \frac{F(\lambda)}{[F_0(\lambda + d\lambda)/F_0(\lambda)]}$$

Where F is the measured spectrum, F_0 is the solar reference spectrum, λ is the original wavelength grid of F, and $\lambda + d\lambda$ is the new wavelength grid. In Bucsela et al. (2006) the irradiance spectrum is interpolated onto the radiance wavelength grid, whereas in our work we interpolate the radiance onto the irradiance wavelength grid to match what is done for the OMI and TROPOMI L2 products.

This method is an improvement over other approaches (e.g. linear or spline) as it reduces interpolation errors related to the sampling rate. However, this improvement is not expected to be significant for instruments like OMI and TROPOMI where undersampling is not a problem. We have updated the text with this clarification.

Pg. 5, line 123: this introductory paragraph is a bit misleading. To my understanding the critical aspect of selecting appropriate spectral channels for NO_2 fitting is not related to the complexity of the radiative transport, but only to the nature of the differential cross-sections and the presence of interfering species.

We agree with your assessment in the case of traditional DOAS NO_2 fits. However, discrete-wavelength DOAS is more sensitive to scattering and albedo effects than traditional DOAS because the polynomial models the broadband component of the reflectance less accurately. This is why the fitting interval must be narrow enough to minimise the effect of the broadband component. The cross sections and the interfering species are still key aspects but in the case of discrete-wavelength DOAS the complexity of the radiative transport also plays an important role. Nonetheless, we acknowledge that the paragraph is misleading and have updated it.

Pg. 5, line 131: replace "mean optical depth" by "differential optical depth" (or difference in optical depth)

Corrected to "differential optical depth".

Pg. 6, Figure 2: how important is it to include liquid water cross-sections in the fitting? In the spectral range of interest, this cross-sections seem to be very unstructured and may correlate strongly with the polynomial function.

We did some tests and concluded that including the liquid water cross section does not make much difference. However, we included it in the fit to match the reference retrieval settings as closely as possible.

Pg. 6, line 144 (very minor comment): the choice of "discrete wavelength DOAS" as a name could in fact be questioned, since fundamentally all DOAS schemes use discrete wavelengths (it is just that in your case, their number is smaller)

We agree, good point. We considered different names and concluded that "discrete-wavelength DOAS" was the one that best described the retrieval approach while still being clear and short. Nonetheless, we welcome suggestions for alternative names that might be more suitable.

Pg. 9, line 199: how can local variations in surface albedo explain differences between retrievals from same satellite pixels? Please clarify the meaning of this statement.

As we discuss in a previous comment, discrete-wavelength DOAS is more sensitive to albedo effects than traditional DOAS. Therefore, we think that one possible explanation for the bigger retrieval differences in the smaller pixels might be related to the different sub-pixel variability of the albedo due to the size of the pixel. In other words, we would generally expect less albedo variability within smaller pixels and this might mean that some stronger spectral features might be present compared to the bigger pixels. These strong spectral features would result in higher retrieval differences between DW-DOAS and the reference level 2 products. We have clarified this in the text.

Pg. 13, Figure 5: why such a discontinuity in the NO_2 map of 30 Oct 2005 (at 20ºS)?

This discontinuity is also present in the reference QA4ECV NO_2 Level 2 product (see http://temis.nl/airpollution/no2col/no2regioomi_qa.php?Region=9&Year=2005&Month=10&Day=30).
We don't exactly know what causes it but it is not present in the tropospheric NO_2 column map, so it is likely a combination of stratospheric NO_2 and processes/elements involved in the air mass factor (AMF) calculation such as atmospheric scattering.

References:

Bucsela, E., Celarier, E., Wenig, M., Gleason, J., Veefkind, J., Boersma, K., and Brinksma, E.: Algorithm for NO_2 vertical column retrieval from the ozone monitoring instrument, IEEE Transactions on Geoscience and Remote Sensing, 44, 1245, https://doi.org/10.1109/TGRS.2005.863715, 2006.

Dekemper, E., Vanhamel, J., Opstal, B. V., and Fussen, D.: The AOTF-based NO_2 camera, Atmospheric Measurement Techniques, 9, 6025– 6034, https://doi.org/10.5194/amt-9-6025-2016, 2016.

Krijger, J. M., van Weele, M., Aben, I., and Frey, R.: Technical Note: The effect of sensor resolution on the number of cloud-free observations from space, Atmos. Chem. Phys., 7, 2881–2891, https://doi.org/10.5194/acp-7-2881-2007, 2007.

Loyola, D. G., Gimeno García, S., Lutz, R., Argyrouli, A., Romahn, F., Spurr, R. J. D., Pedergnana, M., Doicu, A., Molina García, V., and Schüssler, O.: The operational cloud retrieval algorithms from TROPOMI on board Sentinel-5 Precursor, Atmos. Meas. Tech., 11, 409–427, https://doi.org/10.5194/amt-11-409-2018, 2018.

Oldeman, A.: Effect of including an intensity offset in the DOAS NO2 retrieval of TROPOMI, Internship report, R1944-SE, Eindhoven University of Technology/KNMI, Eindhoven, May 2018, https://kfolkertboersma.files.wordpress.com/2018/06/report_oldeman_22052018.pdf, (last access: 10 January 2020), 2018.

Richter, A., Begoin, M., Hilboll, A., and Burrows, J.P.: An improved NO_2 retrieval for the GOME-2 satellite instrument, Atmospheric Measurement Techniques, 4, 1147–1159, https://doi.org/10.5194/amt-4-1147-2011, 2011.

van Geffen, J. H. G. M., Boersma, K. F., Van Roozendael, M., Hendrick, F., Mahieu, E., De Smedt, I., Sneep, M., and Veefkind, J. P.: Improved spectral fitting of nitrogen dioxide from OMI in the 405–465 nm window, Atmos. Meas. Tech., 8, 1685–1699, https://doi.org/10.5194/amt-8-1685-2015, 2015.

Veefkind, J. P., de Haan, J. F., Sneep, M., and Levelt, P. F.: Improvements to the OMI O_2–O_2 operational cloud algorithm and comparisons with ground-based radar–lidar observations, Atmos. Meas. Tech., 9, 6035–6049, https://doi.org/10.5194/amt-9-6035-2016, 2016.

Discrete-wavelength DOAS NO_2 slant column retrievals from OMI and TROPOMI

Cristina Ruiz Villena[1], Jasdeep S. Anand[1], Roland J. Leigh[1,a], Paul S. Monks[2], Claire E. Parfitt[3], and Joshua D. Vande Hey[1]

[1]Department of Physics and Astronomy, Earth Observation Science Group, University of Leicester, Leicester, UK
[2]Department of Chemistry, University of Leicester, Leicester, UK
[3]Thales Alenia Space UK Ltd, Bristol, UK
[a]now at: EarthSense Systems Ltd, Leicester, UK

Correspondence: Cristina Ruiz Villena (crv2@leicester.ac.uk), Joshua Vande Hey (jvh7@leicester.ac.uk)

Abstract. The use of satellite NO_2 data for air quality studies is increasingly revealing the need for observations with higher spatial and temporal resolution. The study of the NO_2 diurnal cycle, global sub-urban scale observations, and identification of emission point sources are some examples of important applications not possible at the resolution provided by current instruments. One way to achieve increased spatial resolution is to reduce the spectral information needed for the retrieval, allowing both dimensions of conventional 2-D detectors to be used to record spatial information.

In this work we investigate the use of ten discrete wavelengths with the well-established Differential Optical Absorption Spectroscopy (DOAS) technique for NO_2 slant column density (SCD) retrievals. To test the concept we use a selection of individual OMI and TROPOMI Level 1B swaths from various regions around the world which contain a mixture of clean and heavily polluted areas. To discretise the data we simulate a set of Gaussian optical filters centred at various key wavelengths of the NO_2 absorption cross section. We perform SCD retrievals of the discrete data using a simple implementation of the DOAS algorithm and compare the results with the corresponding Level 2 SCD products, namely QA4ECV for OMI and the operational TROPOMI product.

For OMI the overall results from our discrete-wavelength retrieval are in very good agreement with the Level 2 data (mean difference < 5 %). For TROPOMI the agreement is good (mean difference < 11 %), with lower uncertainty owing to its higher signal-to-noise ratio. These discrepancies can be mostly explained by the differences in retrieval implementation. There are some larger differences around the centre of the swath and over water. While further research is needed to address specific retrieval issues, our results indicate that our method has potential. It would allow for simpler, more economic satellite instrument designs for NO_2 monitoring at high spatial and temporal resolution. Constellations of small satellites with such instruments on board would be a valuable complement to current and upcoming high-budget hyperspectral instruments.

1 Introduction

Nitrogen dioxide (NO_2) is a gaseous air pollutant from the NO_x family (NO_x = NO + NO_2) that exists in trace amounts in the atmosphere. Its sources are of natural origin (e.g. lightning, volcanoes, and microbial activity) or a result of anthropogenic

activities (e.g. agricultural biomass burning, fossil fuel combustion). ~~While most~~ Most of the background NO_2 ~~,~~ is in the stratosphere and is produced mainly by natural processes~~, is in the stratosphere, in~~ . However, in polluted areas tropospheric NO_2 is predominant ~~. In these areas the main sources of NO_2~~ and its main sources are anthropogenic emissions, which occur close to the surface in the boundary layer. Other sources of tropospheric NO_2 include microbiological soil emissions and lightning (Wallace and Hobbs, 2006).

The most polluted regions are usually highly industrialised and densely populated urban areas, where the air pollution is complex due to the varied mix of constituents (Monks et al., 2009). There is evidence suggesting that NO_2 is a good proxy for the spatial variability of outdoor air pollution in urban environments (e.g. Levy et al., 2013), making it a suitable indicator of air quality.

NO_2 itself has harmful effects on human health, being associated for example with respiratory damage and premature death (WHO Regional Office for Europe, 2013). Moreover, it indirectly plays a role in the climate as it is a precursor of tropospheric ozone and aerosol, two of the Essential Climate Variables defined by the Global Climate Observing System (GCOS) (WMO, 2011).

There has been a continuous effort, particularly in recent decades, to regulate and monitor the concentrations of air pollutants such as NO_2 with the aim of: a) reducing emissions, and b) putting in place mitigation strategies to minimise the exposure of people to harmful levels. Nonetheless, despite a general decreasing trend on NO_2 concentrations in many locations across the globe, particularly in Europe and the United States (e.g. Castellanos and Boersma, 2012; Russell et al., 2012), the World Health Organisation (WHO) guidelines on air quality (WHO, 2006), and EU legislative limits in the case of Europe (EEA, 2018), are still often exceeded (e.g. DEFRA, 2018). In addition, in other areas of the world such as China and India concentrations of nitrogen oxides continued to rise until less than a decade ago (e.g. Huang et al., 2017; Richter et al., 2005; Hilboll et al., 2017). This highlights that there is still a lot to do to tackle the problem of air pollution and that a reliable, consistent long-term monitoring network is crucial.

There are two main methods for the continuous observation of NO_2 in the atmosphere: *in situ* measurements and ~~space-borne remote sensing~~ remote sensing techniques, which include ground-based and space-borne observations. *In situ* instruments such as chemiluminescence analysers (EPA, 1975; Dunlea et al., 2007) provide more accurate values because they directly measure the air they sample. However, it is not logistically or economically viable to install a large number of these around cities, so measurement points are usually sparse. Low spatial sampling is also a limitation of ground-based remote sensing (e.g. Network for the Detection of Atmospheric Composition Change (NDACC; http://ndaccdemo.org/); Pandonia Global Network (PGN; https://www.pandonia-global-network.org)), but they provide long-term quality observations that can be used to validate satellite measurements. On the other hand, satellite instruments provide global coverage but the spatial and temporal resolution is limited, e.g. ~~13~~ 3.5 km × ~~24~~ 5.5 km (at nadir) once per day for ~~OMI (Levelt et al., 2006)~~TROPOMI (Veefkind et al., 2012) , and retrieving surface concentrations of NO_2 from satellite platforms is not straightforward. Increased spatiotemporal resolution is required to improve the accuracy of emission estimates and pollution forecasts (Ingmann et al., 2012). In addition, spatial resolutions in the range of 1 km × 1 km are needed to identify individual sources.

NO_2 has typically been retrieved from measured Earthshine spectra using the well-established Differential Optical Absorption Spectroscopy (DOAS; Platt and Stutz, 2008) technique for over two decades, since the launch of GOME in 1995 aboard ERS-2 (Burrows et al., 1999). This was followed by SCIAMACHY (Bovensmann et al., 1999) aboard Envisat, OMI (Levelt et al., 2006) aboard Aura, GOME-2 (Munro et al., 2006) aboard MetOp-A, MetOp-B and MetOp-C, and more recently TROPOMI (Veefkind et al., 2012) aboard Sentinel-5P. Out of these, GOME-2, OMI and TROPOMI are still operational, and have a single daily overpass in the morning (GOME-2), or in the afternoon (OMI, TROPOMI). TROPOMI provides the best spatial resolution to date, with a true nadir ground pixel size as small as 3.5 km $\times$ 5.5 km, or 1.8 km $\times$ 1.8 km in the occasionally used zoom mode. Unlike their predecessors, OMI and TROPOMI have two-dimensional detectors that allow them to record multiple across-track viewing angles simultaneously (pushbroom measurement mode). While this mode results in higher spatial resolution, it comes at the cost of more optical complexity.

The DOAS principle relies on the separation of broadband and narrowband components of the reflectance spectrum and can resolve multiple gases simultaneously. DOAS retrievals typically use a few hundred spectral channels to perform the slant column density (SCD) fit for each ground pixel. The need for such a large number of channels requires complex optics, and careful wavelength calibration, for which usually the Fraunhofer lines in a reference solar spectrum are used. In addition, one dimension of the detector must be dedicated to recording all this spectral information.

One way to simplify instrument design and increase spatial resolution is to use a retrieval algorithm with reduced spectral information. The idea of using only a few discrete spectral channels to retrieve atmospheric trace gases has been used extensively for ozone retrievals. One example is the Total Ozone Mapping Spectrometer (TOMS; Heath et al., 1975), first launched in 1978 aboard Nimbus-7, which used pairs of discrete wavelengths in the Huggins band (310 - 340 nm) to retrieve ozone. Its strong, narrow absorption features and limited interference from other atmospheric gases makes ozone a relatively easy species to retrieve using discrete wavelengths. For a weak absorber like NO_2, it is more challenging, but it has also been done using passive techniques, such as the Brewer spectrometer (e.g. Cede et al., 2006; Wenig et al., 2008) and the Visible Nitrogen Dioxide instrument aboard the Solar Mesosphere Explorer (Mount et al., 1984), and active techniques, such as DIfferential Absorption LIDAR (DIAL; e.g. Hains et al., 2010). More recently, Dekemper et al. (2016) developed a new concept of "AOTF-based NO_2 camera" which employs pairs of wavelengths recorded sequentially using an acousto-optical tunable filter (AOTF) to image NO_2 in scenes containing plumes. However, these techniques lack sensitivity (e.g. Brewer) or rely on specific viewing geometries that make them unsuitable for nadir-viewing space applications. For example, the AOTF-based NO_2 camera relies on clear-sky pixels being present in the scene for background subtraction. In addition, the sequential sampling of wavelengths poses a limitation to the speed at which they can be registered, making the retrieval challenging for non-static scenes.

In this work we explore the development, application and performance of a discrete-wavelength NO_2 retrieval algorithm based on DOAS (discrete-wavelength DOAS, DW-DOAS hereafter). Our approach combines the reduction in required spectral information with the advantages of DOAS in removing the effects of surface albedo, scattering, and interfering gases. ~~We~~ As a proof of concept, we perform a feasibility study of the technique using data from OMI and TROPOMI and analyse the differences between our results and the operational Level 2 products. In addition, we discuss the implications of discretising

DOAS and the potential application of our method to a future hypothetical instrument aimed at high-spatial-resolution urban air quality monitoring.

2 Method

2.1 Data sources

2.1.1 Ozone Monitoring Instrument (OMI)

The Ozone Monitoring Instrument (Levelt et al., 2006) is an ultraviolet/visible (UV/VIS) spectrometer and operational since it was launched in 2004 aboard the NASA AURA spacecraft. It is a nadir-viewing instrument and follows a sun-synchronous polar orbit, with a daily local overpass time of 13.45 h. The visible band covers a spectral range of 350-500 nm, with a spectral resolution of 0.63 nm and an average sampling distance of 0.21 nm. OMI has a nadir pixel size of 13 km $\times$ 24 km (13 km $\times$ 12 km in spatial zoom mode), with 60 across-track pixels covering a swath width of 2600 km.

OMI has had good ~~radiometric~~ in-flight performance so far, with only ~0.5 % ~~decrease~~ radiometric degradation in the visible channel in the 15 years it has been operational (Levelt et al., 2018). However, it does have one main issue, known as the "row anomaly" (described in detail in the KNMI OMI website: http://projects.knmi.nl/omi/research/product/rowanomaly-background.php), affecting the quality of the radiance in specific rows of the detector. OMI data from 2009 onwards is affected by this anomaly, although early signs started to be seen in 2007. In the work presented here we use Level 1B data from 2005, which is not affected by the row anomaly.

Several OMI Level 2 NO_2 products have been produced by different institutions (e.g. NASA (Krotkov et al., 2017), KNMI (Boersma et al., 2011)). In this work we use the product released as part of the Quality Assurance for Essential Climate Variables (QA4ECV) project (Boersma et al., 2017), which includes recent improvements in the retrieval algorithm (Boersma et al., 2018; Zara et al., 2018).

2.1.2 TROPOspheric Monitoring Instrument (TROPOMI)

Launched in 2017 aboard ESA's Sentinel-5 Precursor, the TROPOspheric Monitoring Instrument (TROPOMI; Veefkind et al., 2012) is the state of the art in remote sensing of atmospheric composition with heritage from OMI and SCIAMACHY. It is a pushbroom nadir spectrometer like OMI but it also covers the near infrared (NIR) and the shortwave infrared (SWIR). It flies in a sun-synchronous polar orbit with about the same daily local overpass as OMI. The visible band of interest in this study (band 4) covers a spectral range of 405-500 nm, with a spectral resolution of 0.55 nm and a spectral sampling of 0.2 nm. Along with an increased ~~SNR~~signal-to-noise ratio (SNR), one of the major advantages of TROPOMI is its unprecedented spatial resolution of 3.5 km $\times$ 5.5 km, which goes down to 1.8 km $\times$ 1.8 km in zoom mode. Like OMI, the swath width is 2600 km, but TROPOMI has 450 across-track pixels. In this study we use TROPOMI Level 1B data and the operational NO_2 Level 2 product (van Geffen et al., 2018).

2.2 Data processing

2.2.1 Processing chain

We simulate discrete-wavelength data by discretising OMI and TROPOMI Level 1B data using digital Gaussian filters. In addition, the relevant absorption cross sections, solar reference and Ring spectrum, convolved with the corresponding row-dependent slit functions for either OMI or TROPOMI, are discretised. Before applying the filters, all the spectra are interpolated onto the ~~radiance~~ irradiance wavelength grid. ~~This is done using the~~ We use a cubic spline interpolation for the cross sections. For the radiance spectra we use the method employed by Bucsela et al. (2006)~~for the irradiance, and with a cubic splineinterpolation for the other spectra.~~ , which calculates the interpolated spectrum using a high-resolution solar reference spectrum as follows:

$$F(\lambda + d\lambda) = \frac{F(\lambda)}{[F_0(\lambda + d\lambda)/F_0(\lambda)]} \quad (1)$$

Where F is the measured spectrum, F_0 is the solar reference spectrum, λ is the original wavelength grid of F, and $\lambda + d\lambda$ is the new wavelength grid. In Bucsela et al. (2006) the irradiance spectrum is interpolated onto the radiance wavelength grid, whereas in our work we interpolate the radiance onto the irradiance wavelength grid to match what is done for the OMI and TROPOMI L2 products. This method is an improvement over other approaches (e.g. linear or spline) as it reduces interpolation errors related to the sampling rate. However, this improvement is not expected to be significant for instruments like OMI and TROPOMI where undersampling is not a problem.

The spectral fit is performed using a custom-made DOAS retrieval routine written in Python, using fitting parameters as close to those of the operational products as possible. The retrieval is described in more detail in section 2.3. Figure 1 shows a flow diagram of the processing chain.

2.2.2 Selection of the discrete channels

~~Earth radiance spectra are the result of a complex combination of absorption and scattering processes in the light path. This means that there is a great dependency on factors such as atmospheric composition, aerosol optical depth (AOD) and the reflective properties of the surface.~~ When the available spectral information is limited to a few discrete points, the selection of suitable channel parameters is critical for the performance of the retrieval. The nature of the differential cross sections, the presence of interfering species, and other effects such as the surface albedo are key aspects in the channel selection.

In this work we have selected 10 channels in the 425-450 nm spectral region, centred at the wavelengths shown in Figure 2. This wavelength range has previously been used in SCIAMACHY (Bovensmann et al., 1999), GOME-2 (Munro et al., 2006), and some ground-based DOAS retrievals (e.g. Vandaele et al., 2005), because it contains strong NO_2 absorption lines. Each channel is modelled as a symmetric Gaussian function defined by three parameters: centre wavelength, full width at

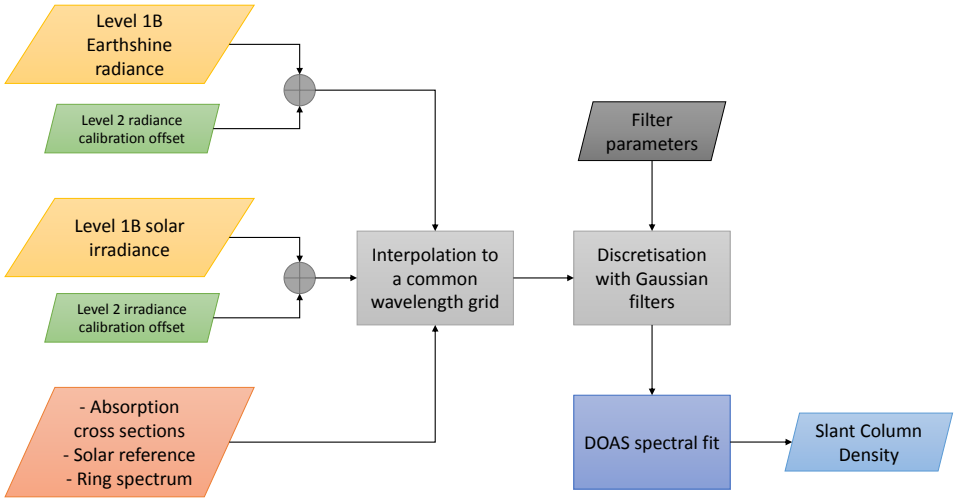

Figure 1. Flow diagram of the data processing used prior to the DW-DOAS retrieval.

half maximum (FWHM), and transmission peak. For this study, we consider only ideal filters (i.e. 100 % transmission), and a FWHM of 1 nm. The criteria for the wavelength selection applied in this work are as follows:

- *Select wavelengths at maxima and minima of the NO_2 absorption cross section, maximising the ~~mean~~ differential optical depth.*
- *Avoid wavelengths where there are large absorptions by interfering species.* While traditional DOAS solves this problem by fitting multiple species simultaneously, this benefit no longer exists when only a few discrete spectral points are available. Water vapour, O_2-O_2 and the Ring spectrum represent the largest interferences in the spectral region of interest.
- *Minimise the total width of the spectral window.* DOAS retrievals can provide different results depending on the spectral window used in the fit (e.g. Alvarado et al., 2014). This owes to the fact that different spectral regions contain unique features which might not be removed properly in the fit. For instance, Richter et al. (2011) found that when they increased the length of the fitting window to obtain higher SNR, unexplained spectral features appeared which were later shown to correspond to sand and liquid water signatures. This demonstrates that a short fitting window minimises the chances of unwanted spectral features. Moreover, it means that a lower order polynomial can be used in the DOAS fit.

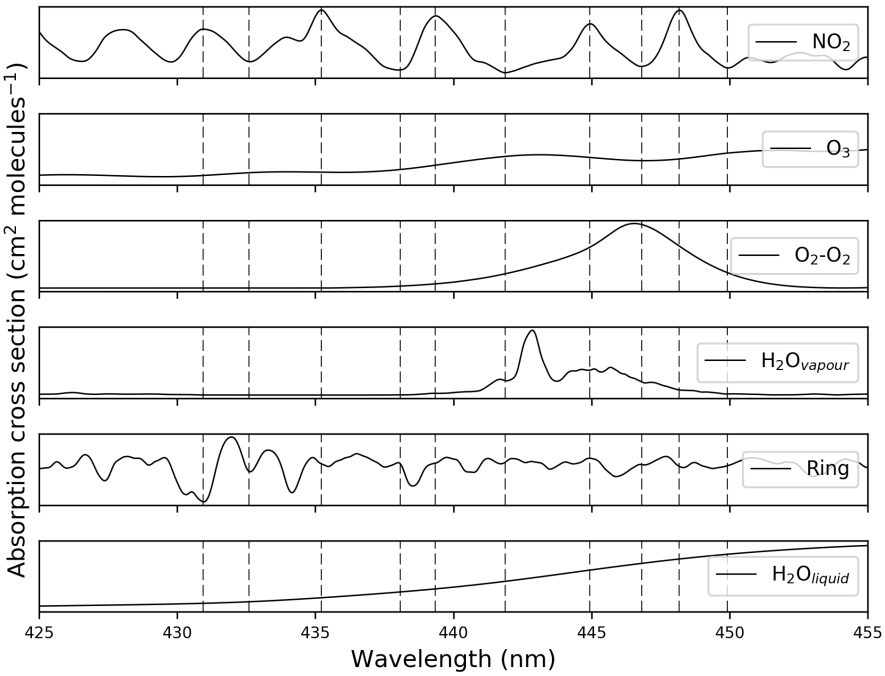

Figure 2. Absorption cross sections of relevant species (solid lines) and position of selected wavelengths (dashed lines) for this study.

2.3 Retrieval

2.3.1 Algorithm description

The retrieval algorithm used in this study is based on elements of DOAS (Platt and Stutz, 2008). There are different implementations of the DOAS technique, mainly the intensity fit (non-linear), and the optical density fit (linear). In DW-DOAS we use the linear approach to obtain the slant column density:

$$\sum_i \sigma_i(\lambda) \cdot N_{s,i} + P(\lambda) = -\ln\left(\frac{I(\lambda)}{I_0(\lambda)}\right) \tag{2}$$

where σ_i is the absorption cross section of the i species fitted, including the Ring spectrum as a pseudo-absorber (Chance and Spurr, 1997); $N_{s,i}$ are the slant column densities; $P(\lambda)$ is a low-order polynomial; $I(\lambda)$ is the Earth radiance; and $I_0(\lambda)$ is the solar irradiance. Since this equation needs to be solved for each wavelength, the resulting problem is a system of equations. This can be represented with the following linear expression:

$$\mathbf{A} \cdot \mathbf{x} = \mathbf{B} \tag{3}$$

$$\begin{bmatrix} \sigma_{NO_2}(\lambda_1) & \sigma_{O_3}(\lambda_1) & \cdots & 1 & \lambda_1 & \lambda_1^2 \\ \sigma_{NO_2}(\lambda_2) & \sigma_{O_3}(\lambda_2) & \cdots & 1 & \lambda_2 & \lambda_2^2 \\ \vdots & \vdots & \ddots & \vdots & \vdots & \vdots \\ \sigma_{NO_2}(\lambda_{10}) & \sigma_{O_3}(\lambda_{10}) & \cdots & 1 & \lambda_{10} & \lambda_{10}^2 \end{bmatrix} \cdot \begin{bmatrix} N_{s,NO_2} \\ N_{s,O_3} \\ \vdots \\ c \\ b \\ a \end{bmatrix} = \begin{bmatrix} -\ln(\frac{I(\lambda_1)}{I_0(\lambda_1)}) \\ -\ln(\frac{I(\lambda_2)}{I_0(\lambda_2)}) \\ \vdots \\ -\ln(\frac{I(\lambda_10)}{I_0(\lambda_10)}) \end{bmatrix} \tag{4}$$

where ~~A is an $M \times N$~~ $\mathbf{A}$ is an M × N matrix containing the absorption cross sections and the polynomial basis for each wavelength, ~~x is a row vector of N~~ $\mathbf{x}$ is a column vector of N elements containing the slant column densities of the absorbers ($N_{s,i}$) and the polynomial coefficients (a, b, c), and ~~B~~ $\mathbf{B}$ is a column vector of ~~M~~ M elements containing the optical density for each wavelength. In order to solve for ~~x~~ $\mathbf{x}$ we calculate the pseudo inverse of matrix ~~A, namely A^{-1}~~ $\mathbf{A}$, namely $\mathbf{A}^{-1}$, using the Singular Value Decomposition (SVD) numerical method to factorise ~~A~~ $\mathbf{A}$:

$$\mathbf{A} = \mathbf{U} \cdot \mathbf{W} \cdot \mathbf{V}^T \tag{5}$$

$$\mathbf{A}^{-1} = \mathbf{V} \cdot \mathbf{W}^{-1} \cdot \mathbf{U}^T \tag{6}$$

where ~~U is an $M \times N$~~ $\mathbf{U}$ is an M × N column-orthogonal matrix, ~~W is an $M \times N$~~ $\mathbf{W}$ is an M × N diagonal matrix with non-negative real numbers in the diagonal (singular values), and ~~V is an $N \times N$~~ $\mathbf{V}$ is an N × N orthogonal matrix.

Although this approach is similar to a traditional DOAS retrieval, there are some differences arising from having only a few discrete spectral points. First, the order of the polynomial must not be greater than 2, as fitting higher order polynomials results in erroneously low slant column densities. In a way, this limits one of the key advantages of DOAS, this is, the ability to remove the broadband part of the reflectance. However, this can be overcome by having a fitting window narrow enough that the broadband component can be approximated by a 2nd-order polynomial, and is one of the criteria used in this work for wavelength selection (see Section 2.2.2). The concept of 'fitting window' in the context of DW-DOAS should be interpreted as a spectral range that contains the discrete wavelengths rather than in a literal sense as is the case for hyperspectral DOAS retrievals.

Another consequence of discretising the spectra is that it is no longer possible to perform a wavelength calibration using the Fraunhofer lines of the solar reference spectrum. Therefore, no wavelength calibration is done as part of the retrieval. The implications of this limitation for a future operational instrument are discussed in Section 3.5.

The last difference between discrete and traditional DOAS is related to the ability to perform a "shift and squeeze" to correct for small spectral misalignments. In traditional DOAS two additional non-linear coefficients can be fitted to correct the spectra in this manner. This cannot be done in the context of a discrete-wavelength retrieval owing to the lack of spectral information available, so such parameters are not fitted.

Table 1. NO_2 SCD retrieval details for OMI and TROPOMI reference products and DW-DOAS.

	OMI QA4ECV (v 1.1) (Boersma et al., 2018)	TROPOMI (van Geffen et al., 2019a, b)	DW-DOAS (this work)
Fitting window	405 - 465 nm	405 - 465 nm	~~430~~ 425 - 450 nm
Fitting method	Optical depth (linear)	Intensity (non-linear)	Optical depth (linear)
χ^2 minimisation method	Levenberg-Marquardt	Optimal Estimation	Not applicable
Level 1B uncertainty in χ^2	No	Yes	Not applicable
Selection reference spectrum	Annual mean (2005) solar reference	Daily solar reference	Same as reference product (annual mean/daily solar reference)
Polynomial degree	4	5	2
Intensity offset correction	Constant	No	No
Fitting parameters	O_3, NO_2, O_2-O_2, H_2O_{vap}, Ring, H_2O_{liq}, I_{off}, shift and stretch	O_3, NO_2, O_2-O_2, H_2O_{vap}, H_2O_{liq}, shift	O_3, NO_2, O_2-O_2, H_2O_{vap}, Ring, H_2O_{liq} (only TROPOMI)
Treatment of Ring effect	Pseudo-absorber	Non-linear fit	Pseudo-absorber
Wavelength calibration (radiance)	Along with fit, 405-465 nm	Before fit, 405-465 nm	No
Temperature	220 K	221 K	Same as reference product (220 K/221 K)

Table 1 shows a comparison between our discrete-wavelength retrieval and the algorithms used for TROPOMI and OMI QA4ECV.

2.3.2 Retrieval uncertainty

The retrieval uncertainty is estimated using a method commonly employed as an independent evaluation of DOAS SCD uncertainty estimations (e.g. Zara et al., 2018; Boersma et al., 2007). The method calculates the uncertainty as the spatial variability of the SCD over a remote area in the Pacific Ocean which is considered to have background NO_2 concentrations. The assumption is that the variation in the NO_2 SCDs is caused solely by the retrieval uncertainty, therefore, this can be calculated as the standard deviation of spatial spread of SCDs. The area selected corresponds to latitudes between 60° S and 60° N, and longitudes between 150° W and 180° W. To account for light path differences the area is divided into 2° × 2° boxes so that the

pixels in each box can be assumed to have similar path lengths. The geometric air mass factor (AMF) is used as an indicator of the path length for each pixel; a good description of AMFs can be found in Palmer et al. (2001). Boxes with high geometric air mass factor (AMF) variability (> 5 %) are discarded. The relative AMF variability is calculated using the expression defined in (Zara et al., 2018):

$$AMF_{var} = \frac{\sqrt{(\overline{M_i^2} - \overline{M_i}^2)}}{M_i} \tag{7}$$

Where M_i is the geometric AMF of each pixel (i) within one box, calculated as a function of the solar zenith angle (θ_s) and the satellite viewing angle (θ_v):

$$M_i = \sec\theta_{s,i} + \sec\theta_{v,i} \tag{8}$$

Then we calculate the deviation of each pixel from its box SCD mean and fit a Gaussian to the results, from which we obtain the standard deviation corresponding to the SCD uncertainty.

3 Results and discussion

3.1 OMI NO_2 SCD comparison

As an initial exercise, the NO_2 SCD results from our DW-DOAS retrieval of selected single orbits from January of 2005 are compared with the corresponding OMI QA4ECV NO_2 product. Figure 3 shows the results from both retrievals and the relative differences between them. The three orbits selected have a mixture of heavily polluted and clean areas with respect to NO_2. In all three swaths the datasets are highly correlated, with DW-DOAS generally producing lower NO_2 SCDs (~5 %). The largest differences are found around the centre of each swath, which coincides with the areas with the lowest SCDs in the QA4ECV dataset. These areas also are around the equator, where the geometric light paths are shortest. Furthermore, the middle of the swath is where ground pixel sizes are smallest. DW-DOAS is more susceptible to albedo effects than traditional DOAS, so the ~~SCDs may be more susceptible to local variations in surface albedo.~~ higher differences might be related to the sub-pixel variability of the albedo. Smaller pixels have lower variability and this might mean that some stronger spectral features might be present that cause higher errors.

It is visually apparent from Figure 3 that DW-DOAS results are slightly noisier than those retrieved by QA4ECV, particularly over unpolluted areas. This is expected given the limited spectral information available for the retrieval and indicates a lower sensitivity to NO_2 of DW-DOAS compared to hyperspectral retrievals. This difference in noisiness is quantified in the statistical uncertainty estimation (Section 3.3).

The differences between DW-DOAS and QA4ECV SCDs are normally distributed, as shown in the histograms in Figure 4. However, the negative biases indicate systematic differences between datasets, which are likely due to differences in retrieval

implementation and settings. These biases are within the anticipated values from relevant sensitivity studies from the literature, which are summarised in Table 1. The main differences stem from the absence of wavelength calibration in the case of DW-DOAS, the inclusion of an intensity offset in the fit in the case of QA4ECV, and the differences in the fitting window. Different spectral regions may contain spectral signatures that are not accounted for in the retrieval, which can cause biases when different fitting windows are used (e.g. van Geffen et al. (2015)). Also in Figure 4 are the correlation plots for all the selected swaths. These corroborate the good agreement between datasets that is evident in Figure 3, with $r > 0.99$ in all cases.

In order to check for any geographical and seasonal variabilities in the results we processed all single orbits from 4 days in January, April, July and October of 2005. The results can be seen in Figure 5, which shows the DW-DOAS retrieval results (scaled with the geometric AMF for clarity) and the relative differences with the QA4ECV product. Maps of the absolute differences can be found in Appendix A. Similar patterns to those seen in Figure 3 for individual orbits are also seen in the global maps of relative differences. The largest differences are seen mainly around the equator and they are highest in the April data. However, these features seem to be a result of using relative differences with small values and are not present to the same extent in the maps of absolute differences (Figure A1). Some of the differences observed over the ocean could be attributed to the intensity offset correction that is included in the QA4ECV product. The physical meaning of this term is not well understood, but it is included in the retrieval to account for spectral signatures caused by vibrational Raman scattering over water and incomplete Ring corrections, and to prevent O_3 misfits (Boersma et al., 2018).

Some of the lowest differences are found in large plumes of NO_2, for example, in North America and China in the January map. Two other interesting features stand out from the global maps. Firstly, DW-DOAS seems to consistently underestimate the SCDs over the Sahara desert, which is likely due to the spectral signature of sand. It could be argued that it is the high albedo of the desert causing higher errors, but this only seems to happen significantly over that area. The second feature is found in South America around 30° S, where there is an area of higher differences between retrievals. This is also apparent on the SCD maps, and seems to coincide with the region affected by the South Atlantic Anomaly (SAA), which is known to affect DOAS retrievals (e.g. Richter et al., 2011). The OMI QA4ECV product includes a spike correction that significantly reduces the scatter in the area affected by the SAA, which might explain the differences.

Figure 6 shows the correlation plots for DW-DOAS and QA4ECV using the global NO_2 SCD data from Figure 5. The agreement between datasets when using global data is reduced owing to spatial features in the differences, as discussed previously. There are more outliers in the data from April and July, and most of them correspond to lower slant column densities and lower cloud radiance fractions. In fact, some of the spatial features that can be seen in Figure A1 seem to correspond to cloud structures, with lower differences over cloudy pixels. For cloud-free pixels effects such as the surface albedo or lower SNRs, as well as vibrational Raman scattering over water (Oldeman, 2018), might be contributing to the higher differences.

3.2 TROPOMI NO_2 SCD comparison

To extend the analysis we performed a similar analysis to that done for OMI, described in section 3.1, using data from the TROPOMI NO_2 operational product. First, the results from DW-DOAS for 3 selected orbits from 31/01/2019 are compared to the operational product (see Figure 7). As was the case for OMI, there is high correlation between the datasets, with DW-

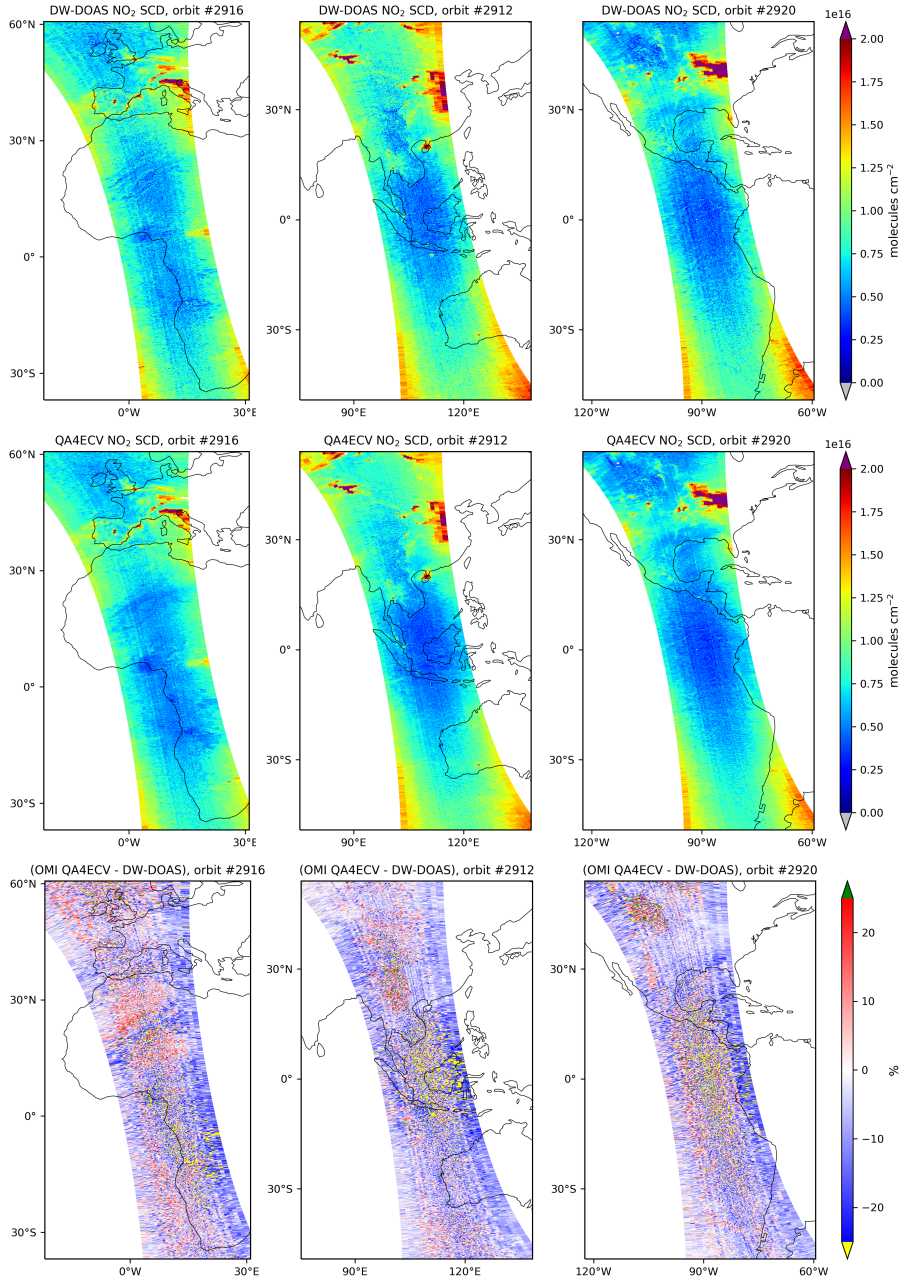

Figure 3. (top) NO_2 SCDs retrieved by DW-DOAS for selected orbits of 31/01/2005 in all-sky conditions, (middle) corresponding QA4ECV NO_2 SCDs, and (bottom) the relative differences between them calculated as (QA4ECV - DW-DOAS)/QA4ECV and expressed in %.

DOAS producing SCDs ~11 % smaller than TROPOMI. The largest differences are located towards the centre of the swath and

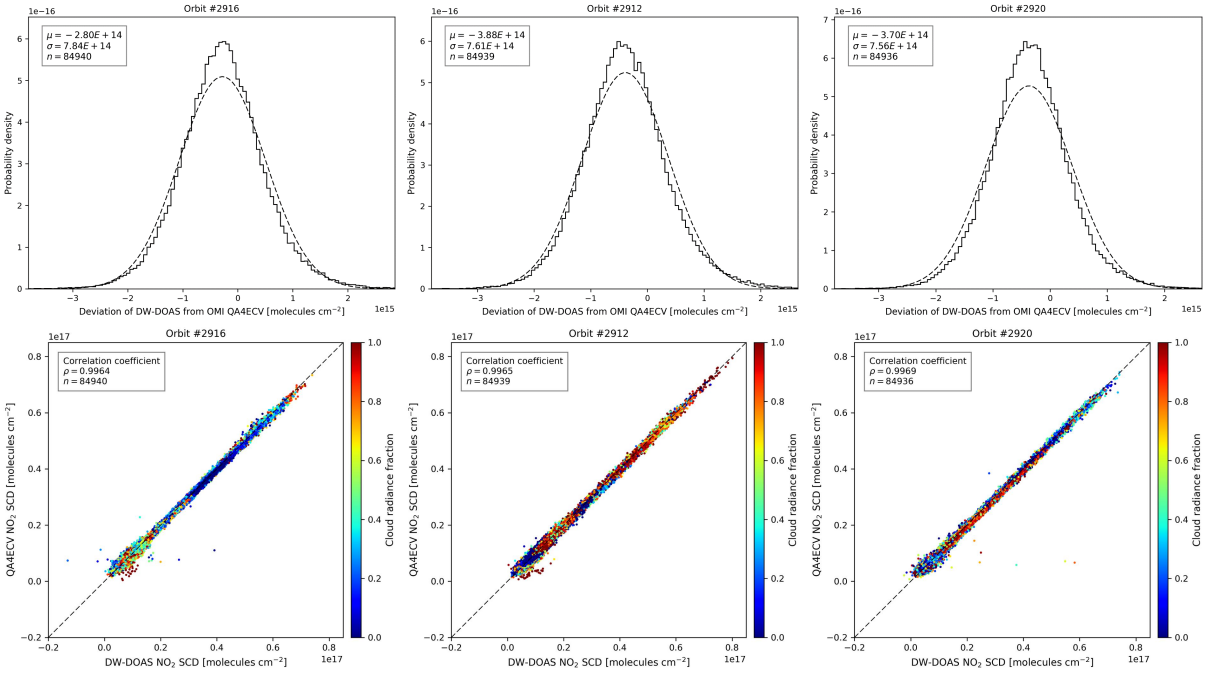

Figure 4. (top) Distribution of absolute differences between the NO_2 SCDs retrieved by DW-DOAS and QA4ECV for the orbits in Figure 3, calculated as (QA4ECV – DW-DOAS), and (bottom) corresponding correlation plot.

Table 2. Anticipated SCD differences between QA4ECV and DW-DOAS due to retrieval implementation differences, based on the literature.

	OMI QA4ECV	DW-DOAS	Anticipated SCD difference (QA4ECV - DW-DOAS)	Motivation
Fit window	405-465 nm	425-450 nm	$+0.5 \times 10^{15}$ molec. cm^{-2}	Figure 11 in van Geffen et al. (2015)
Intensity offset	Yes	No	$\pm$ 0.3 $\times 10^{15}$ molec. cm^{-2} (depends on land vs ocean)	Figure 3(b) Boersma et al. (2018)
Wavelength calibration	Yes	No	-0.85 $\times 10^{15}$ molec. cm^{-2}	van Geffen et al. (2015)
Net anticipated effect:	(QA4ECV - DW-DOAS) = (0.5 + ($\pm$ 0.3) - 0.85) $\times 10^{15}$ = (-0.35$\pm$ 0.3) $\times 10^{15}$ molecules cm^{-2}			

coincide with the lowest SCDs in the TROPOMI operational product. As with OMI data, the differences are smaller in areas with high SCDs.

Figure 8 shows the histograms of the differences between retrieval results, and the correlation plots. These are similar to those obtained for OMI, and indicate that the differences are normally distributed and that the correlation is better than 0.99. However, in the case of TROPOMI the biases are much larger. Nonetheless, these still fall within the range of expected

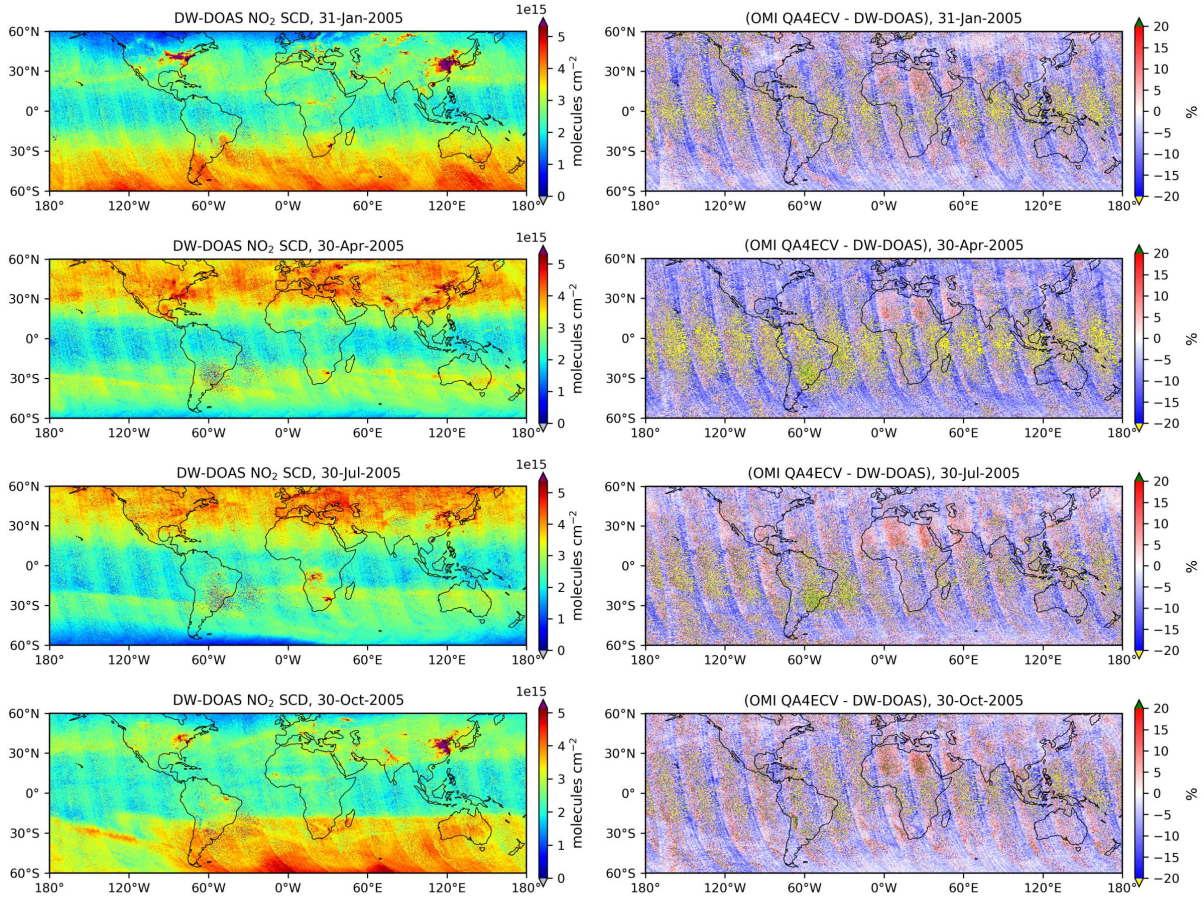

Figure 5. (left) Global DW-DOAS NO_2 SCDs scaled with geometric AMFs (for clearer data visualisation) for all single orbits of one day in January, April, July and October of 2005, and (right) the relative differences with QA4ECV calculated as (QA4ECV – DW-DOAS)/QA4ECV and expressed in %. The latitudes are limited to [60° S, 80° N]. Data from all-sky conditions have been used.

differences in SCD related to retrieval implementation and settings. Table 3 contains the expected range of SCD differences according to the literature. The main contributions are from differences in fitting window, the inclusion of an intensity offset in the case of TROPOMI, and the different implementation of DOAS (non-linear in the case of TROPOMI, and linear in the case of DW-DOAS). Interestingly, although the biases are higher than in the case of OMI, the standard deviation of the differences between DW-DOAS and TROPOMI is smaller owing to its higher intrinsic SNR.

Figure 9 shows the global maps of SCDs retrieved by DW-DOAS and their relative differences with the TROPOMI operational product. Maps of the absolute differences can be found in Appendix A. The patterns in the single orbits are also seen throughout the global data. The largest relative differences are generally found in central across track pixels and are smaller at the edges of the swaths. While for OMI these were found around the equator, for TROPOMI they are spread further along the swaths, and are more pronounced over water. As it was the case with OMI, large relative differences are not as strong on

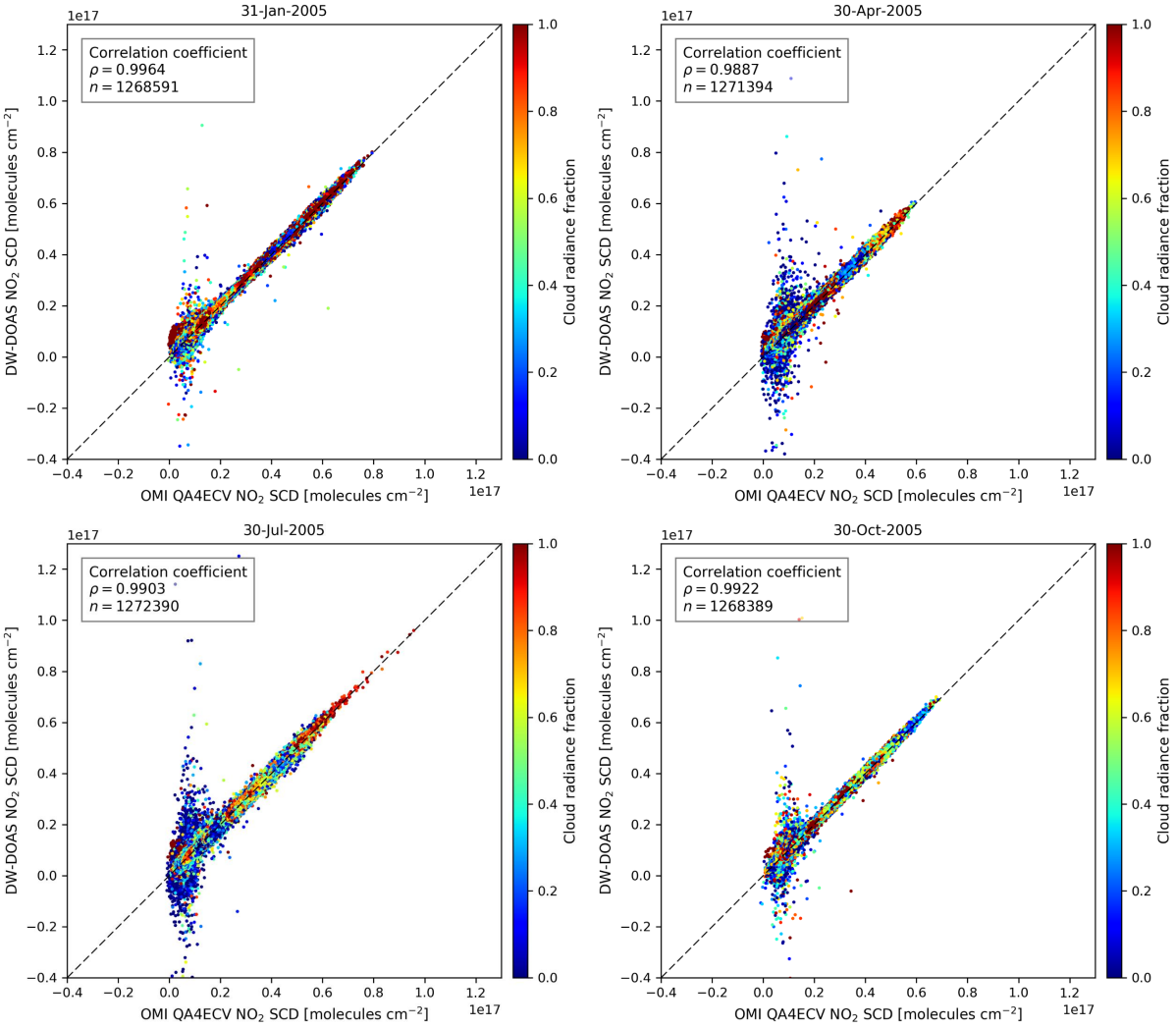

Figure 6. Correlation plots of DW-DOAS and QA4ECV global NO_2 SCD data used in Figure 5.

the maps of absolute differences (Figure A1) and they are thought to be partly the result of small SCD values. Interestingly, most of the areas with the largest differences coincide with high liquid water SCDs from the TROPOMI NO_2 level 2 operational product (retrieved as part of the DOAS fit; not shown here). It is ~~unclear~~ not completely clear what causes these spatial patterns, but surface albedo, cloudiness, smaller pixel sizes and viewing geometry might play a role. Over land the differences are generally lower, with the exception of the Sahara desert. Unlike for OMI, for TROPOMI the effect of the SAA is not as obvious from the SCD maps, but it can be seen to a lesser extent in the maps of differences.

The global correlation plots in Figure 10 show similar correlation coefficients as those seen for OMI. However, once again the increased SNR is reflected in the standard deviation of the SCD differences, particularly for lower values, where it is

Table 3. Anticipated SCD differences between TROPOMI and DW-DOAS owing to retrieval implementation differences, based on the literature.

	TROPOMI	DW-DOAS	Anticipated SCD difference (TROPOMI - DW-DOAS)	Motivation
Fit window	405-465 nm	425-450 nm	+0.5 $\times$ 10^{15} molec. cm^{-2}	Figure 11 in van Geffen et al. (2015)
Intensity offset	Yes	No	-0.85 $\times$ 10^{15} molec. cm^{-2}	van Geffen et al. (2015)
Fit method	Intensity fitting	Optical density	+0.2 $\times$ 10^{15} molec. cm^{-2} (over Africa)	Figure 3(a) Boersma et al. (2018)
Net anticipated effect:	(TROPOMI - DW-DOAS) = (0.5 + ($\pm$ 0.3) + 0.2) $\times$ 10^{15} = (0.7 $\pm$ 0.3) $\times$ 10^{15} molecules cm^{-2}			

markedly smaller than that obtained for OMI. There are fewer outliers and, unlike for OMI, they mostly correspond to pixels with high cloud radiance fraction. The dependence on cloud radiance fraction for both instruments cannot be directly compared, because the OMI and TROPOMI observations are over a decade apart and so will be subject to very different cloud structures. Additionally, TROPOMI has a smaller pixel size and so will experience very different cloud radiance fractions to OMI (Krijger et al., 2007). Finally, there may also be inherent differences between the cloud top heights observed by both instruments based on the different retrieval algorithms they employ; OMI retrieves this parameter using the O_2-O_2 absorption feature at 477 nm (Veefkind et al., 2016), while TROPOMI makes use of the O_2-A band in its operational retrieval (Loyola et al., 2018). In addition, the QA4ECV product for OMI includes an intensity offset correction, which is not included in the TROPOMI product, and that may explain some of the differences over the ocean (Oldeman, 2018).

3.3 SCD uncertainty estimation

We apply the method described in Section 2.3.2 to calculate the NO_2 SCD statistical uncertainty for DW-DOAS for OMI and TROPOMI, including all the boxes in the region of interest for all four seasons. In order to validate our estimates, we also apply the method to the reference datasets, namely the OMI QA4ECV and TROPOMI operational products, and compare the results. The calculations only include boxes with low geometric AMF variability (< 5 %). An example of the distribution of the deviation of the SCDs from their respective box mean for the January datasets is shown in Figure 11, and Table 4 contains the average results for all seasons. In all cases DW-DOAS gives higher uncertainty than the reference level 2 datasets, with this difference being more pronounced for OMI data. TROPOMI histograms have a better Gaussian fit, partly due to the higher quality of the data, but largely because its higher spatial resolution means there are more pixels for the same area used in the calculation, i.e. a larger sample size.

We also evaluate the sensitivity of DW-DOAS to striping, which is caused by the inhomogeneous illumination of the entrance slit of the instrument (Dobber et al., 2008). This issue is more pronounced in OMI, and it is usually corrected for after the DOAS

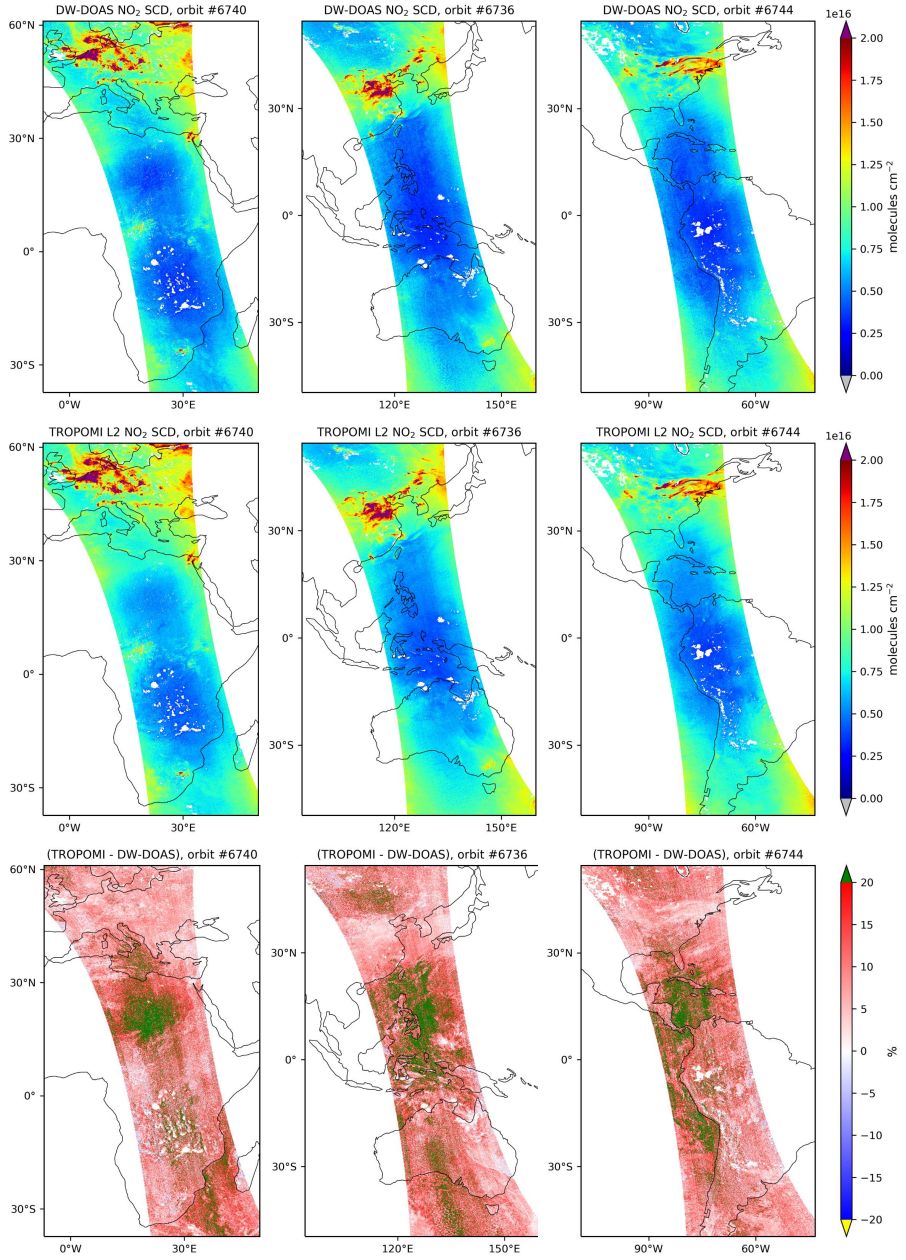

Figure 7. (top) NO_2 SCDs retrieved by DW-DOAS for selected orbits of 31/01/2019, (middle) corresponding TROPOMI NO_2 SCDs, and (bottom) the relative differences between them calculated as (TROPOMI - DW-DOAS)/TROPOMI and expressed in %. All the data are screened using the QA flag (qa > 0.5) from the TROPOMI NO_2 level 2 dataset, which includes all-sky pixels.

retrieval. Figure 12 shows the deviation from the mean SCD scaled with the geometric AMF as a function of across-track pixel number for one orbit over a clean area of the Pacific Ocean. The magnitudes of the peaks and troughs indicate that DW-DOAS

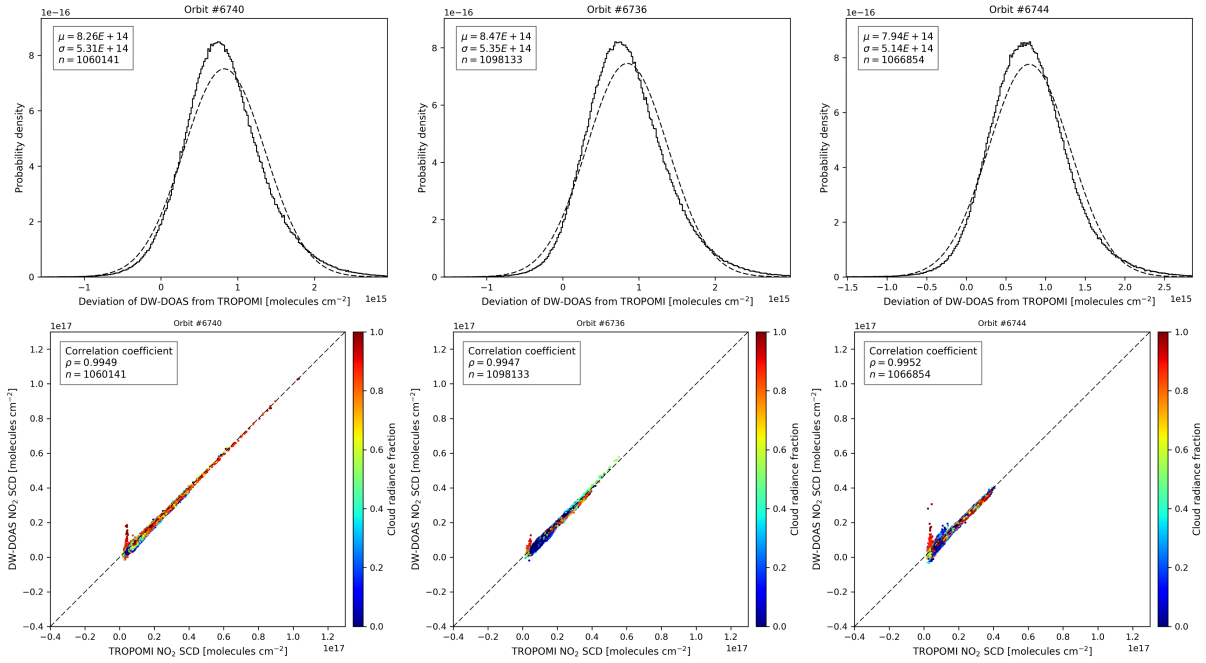

Figure 8. (top) Distribution of absolute differences between the NO_2 SCDs retrieved by DW-DOAS and TROPOMI for the orbits in Figure 7, calculated as (TROPOMI – DW-DOAS), and (bottom) corresponding correlation plot.

Table 4. Comparison of mean SCD statistical uncertainties for OMI QA4ECV, TROPOMI, and DW-DOAS, calculated from SCDs from a remote area in the Pacific Ocean within latitudes [60° S, 60° N] and longitudes [180° W, 150° W].

Mean statistical σ ($\times 10^{15}$ molec. cm^{-2})		
Instrument	DW-DOAS	Reference L2 product
OMI	0.97	0.71
TROPOMI	0.68	0.54

has a higher sensitivity to striping compared to OMI QA4ECV, but it is less of an issue for TROPOMI because of the higher quality of the data.

3.4 Method limitations

Some of the challenges of using DW-DOAS for NO_2 come from using limited spectral information to retrieve a relatively weak absorber. One limitation is the increased sensitivity to random noise, as seen in the retrieval results and demonstrated by the SCD statistical uncertainty estimations. Another limitation is the higher sensitivity to interfering species, since there is not

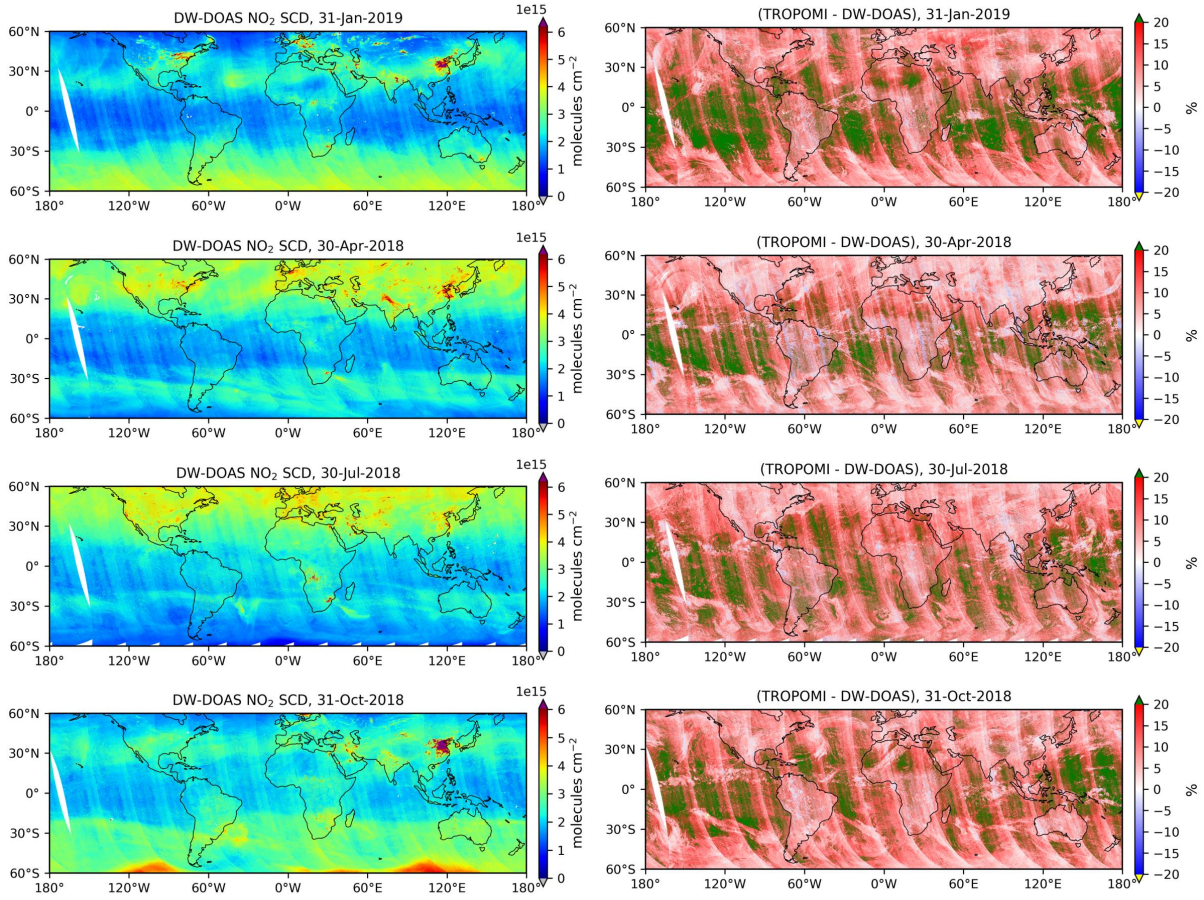

Figure 9. (left) Global DW-DOAS NO_2 SCDs scaled with geometric AMFs (for clearer data visualisation) for all single orbits of one day in January of 2019, and April, July and October of 2018, and (right) the relative differences with TROPOMI calculated as (TROPOMI – DW-DOAS)/TROPOMI and expressed in %. The latitudes are limited to [60° S, 80° N]. All the data are screened using the QA flag (qa > 0.5) from the TROPOMI NO_2 level 2 dataset, which includes all-sky pixels.

enough spectral information to completely separate out the gas of interest from the other species. However, the effect of this can be minimised by optimising the wavelength selection.

Furthermore, DW-DOAS has particular limitations that stem from the use of discrete wavelengths in combination with the DOAS retrieval technique. Firstly, one of the basic premises of DOAS is the removal of broadband structures from the reflectance spectra using a polynomial, typically 4th or 5th order. As explained in section 2.3.1, using a polynomial of such a high degree would cause the retrieval to underestimate the NO_2 SCD, so this is limited to a 2nd-order polynomial. However, sometimes this is not enough to remove complex surface albedo or scattering broadband structures. These residual structures might be the underlying cause behind some of the higher SCD differences between DW-DOAS and the OMI and TROPOMI

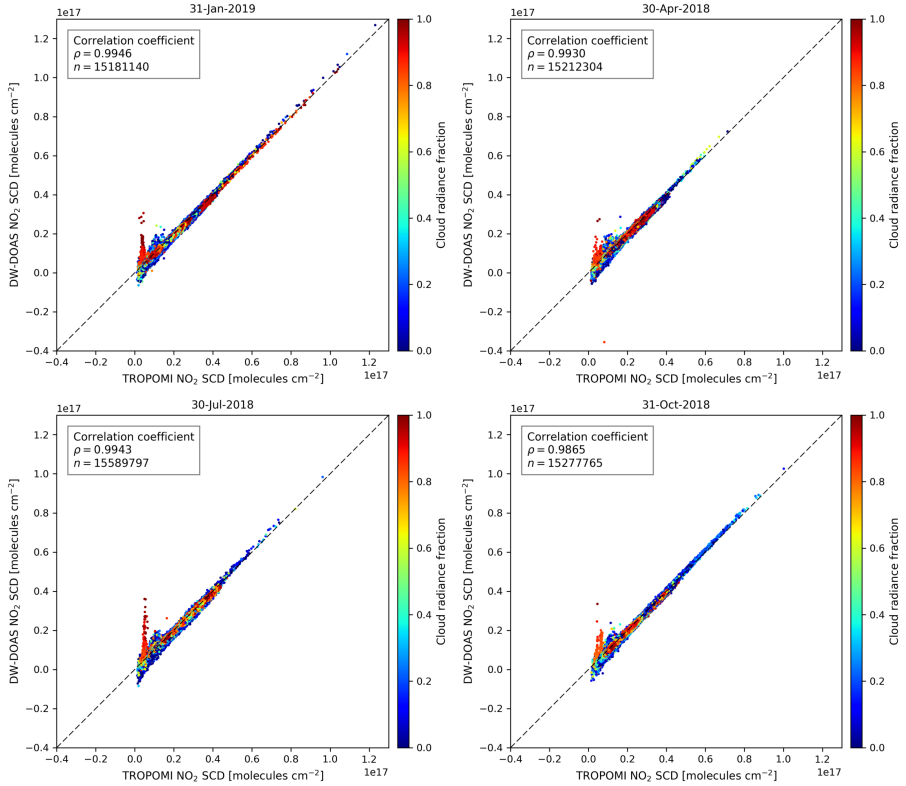

Figure 10. Correlation plots of DW-DOAS and TROPOMI global NO_2 SCD data used in Figure 9.

reference products, and can be minimised by selecting channels that are close together so that they can be approximated by a 2nd-order polynomial.

Finally, wavelength calibration using a high-resolution solar reference is an important step in DOAS retrievals because even a small wavelength shift can cause retrieval errors. With discrete-wavelength data it is not possible to use the Fraunhofer lines of the solar spectrum for the wavelength calibration. While this is a shortcoming, it is anticipated that small wavelength shifts do not have as big an impact as they are for hyperspectral DOAS precisely because the spectral channels are sparse and not contiguous, and because the filters are wider.

3.5 Considerations for future instruments

The DW-DOAS results we have presented are promising and the method has potential to be applied to new satellite instrument designs. However, several aspects need to be considered before it can be implemented in an operational instrument:

- **Reference spectrum.** The DW-DOAS method has only been tested using a solar spectrum as the reference (I_0) for the DOAS fit. However, Earthshine radiance spectra could be used instead, as demonstrated by Anand et al. (2015). Using these spectra would simplify the instrument design by removing the need for a solar diffuser and a solar measure-

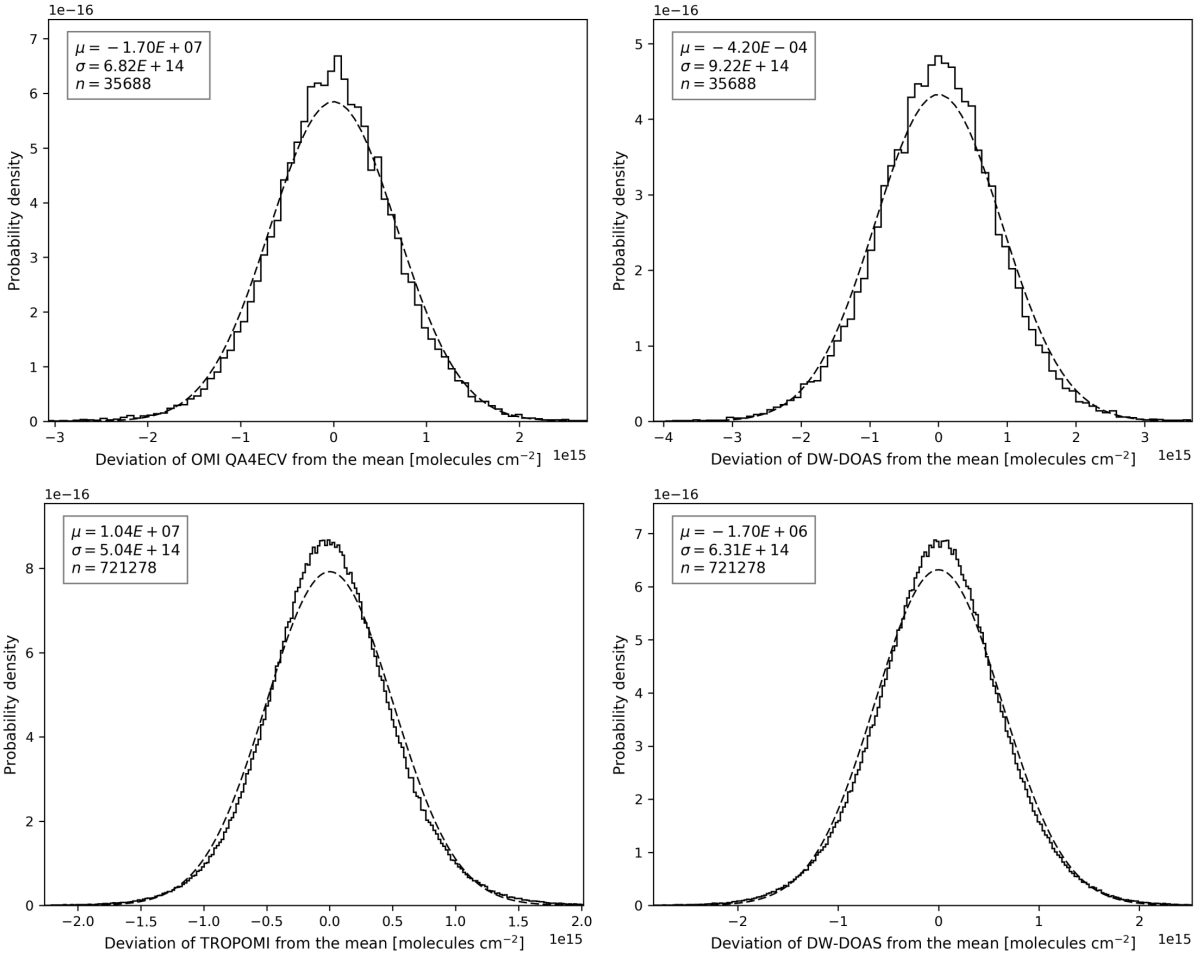

Figure 11. Histogram of the deviation of the NO_2 SCDs from the box mean for OMI (top) and TROPOMI (bottom), for DW-DOAS (right) and the corresponding reference products (left). OMI data has not been screened for clouds; TROPOMI data has been screened using the quality assurance value (qa > 0.5) from the level 2 NO_2 product. The data shown are from January 2005 (OMI) and January 2019 (TROPOMI).

ment mode; it would cancel out some instrumental effects and reduce the effect of the Ring structures in the retrieval. Moreover, in theory a synthetic solar spectrum could also be used. Nevertheless, all options come with drawbacks, so a sensitivity study would be needed to find the approach that provides the best results.

- **Wavelength calibration and filter response function.** As discussed in Section 3.4, it is not possible to perform a wavelength calibration for DW-DOAS using a solar reference spectrum owing to the lack of spectral information. Thus, a mechanism for in-flight monitoring of the spectral response of the filters would be critical, since these need to be known accurately to convolve the absorption cross sections.

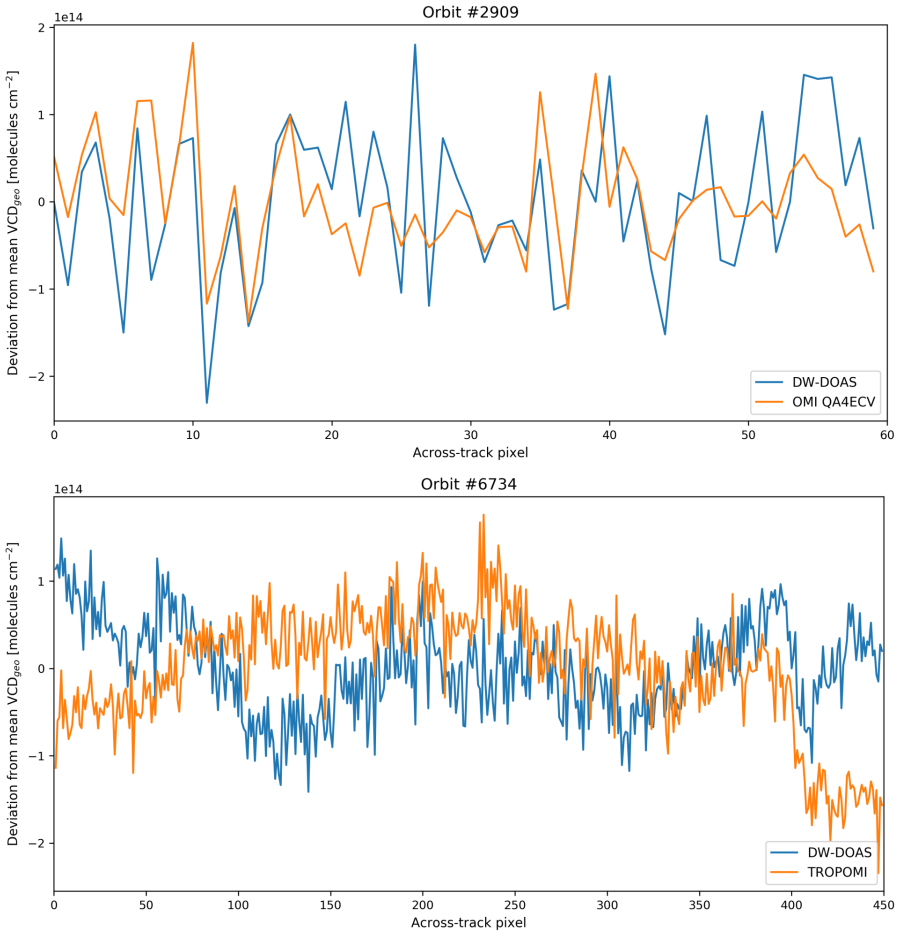

Figure 12. Striping sensitivity of DW-DOAS and the corresponding reference product for (top) OMI and (bottom) TROPOMI data for one orbit over the Pacific Ocean in the latitude range 30° S – 5° N.

- **Cloud retrieval.** To use DW-DOAS operationally a cloud retrieval would be needed to identify cloudy pixels. In other retrieval algorithms using visible spectra this is performed using knowledge of the O_2-O_2 slant column, which can be derived from its absorption cross section peak at ~477 nm (Veefkind et al., 2016). However, it is not possible to retrieve O_2-O_2 with the wavelengths proposed in this work because they are optimised for NO_2. Therefore, further work is needed to find a suitable solution, for example, by adding a few channels to detect the aforementioned O_2-O_2 peak.

- **AMF calculations.** This work has evaluated the performance of the NO_2 SCD retrieval. However, that is only the first of the three steps in an NO_2 tropospheric vertical column retrieval, which is the final product for the typical end user. The other two steps are the stratospheric-tropospheric NO_2 separation (e.g. model assimilation, Boersma et al. (2011)), and the conversion of SCDs into vertical column densities (VCDs) using air mass factors (AMFs; Palmer et al., 2001). These

two steps are mostly independent from the SCD fit, so in principle no major differences are expected for DW-DOAS. However, further work is needed to test these and ensure that any retrieval-dependent sensitivities are understood before DW-DOAS is implemented in an operational instrument. This is particularly true for very high spatial resolutions, where the surface albedo might be a problem for DW-DOAS owing to the polynomial limitation.

4 Conclusions and further work

We have developed a method, DW-DOAS, to perform NO_2 slant column density retrievals using only 10 discrete spectral channels and the DOAS technique. It has been tested using OMI and TROPOMI datasets and found to produce results that are comparable to the reference level 2 products, with a mean difference of ~5 % for OMI QA4ECV and ~11 % for TROPOMI. However, DW-DOAS has higher uncertainties, which are due to a higher sensitivity to noise, and it is more sensitive to striping. While there is a high correlation ($r > 0.99$) of the DW-DOAS results with the reference level 2 products, some spatial variabilities are found. The largest differences are seen over water, ~~near the equator,~~ in the Sahara desert, and in clear-sky areas with low NO_2 SCDs. In addition, the centre of the swath presents higher differences. The cause of these is ~~unknown~~ not completely clear, but low NO_2 concentrations, cloudiness, and short light paths might play a role.

The main advantage of the DW-DOAS method over existing DOAS retrievals is the need for comparatively little spectral information, which makes the retrieval faster and would allow potential instruments designs with high spatial resolution. Limitations of the method include higher sensitivity to broadband structures such as surface albedo; higher sensitivity to noise, which means a higher SNR is required; inability to perform a wavelength calibration using a high-resolution solar reference; and the ability to retrieve only NO_2, although with further work it might be possible to retrieve other species by adding a small number of channels.

Despite the shortcomings, our results show that the DW-DOAS method has potential. It could be used in future satellite instruments to allow simpler designs, for example, by having individual optical channels, each with an optical filter and a detector, instead of the traditional spectrometer with a diffraction grating and mirrors. Two of the main challenges of this kind of approach are the co-registration and cross-calibration of the individual channels. In addition, we anticipate that the requirements of spectral accuracy and stability would be more restrictive, particularly given the narrow bands, the limited number of channels, and the more challenging in-flight calibration (it is not possible to use the Fraunhofer lines). However, a comprehensive sensitivity analysis is required to further assess the operational feasibility of such an instrument concept and derive performance requirements.

DW-DOAS in combination with a simple, compact instrument design could be used in low-cost constellations for air quality monitoring at high resolution. This type of constellation could be a good complement to existing high-budget hyperspectral instruments such as OMI and TROPOMI, for example, for the detection of small scale NO_2 hotspots, which could be identified from space and investigated further using *in situ* instruments. Furthermore, DW-DOAS could potentially be used for faster retrievals (e.g. for near-real time processing) for hyperspectral data from existing instruments. Processing speed is especially important for higher data volumes expected by future high-resolution instruments.

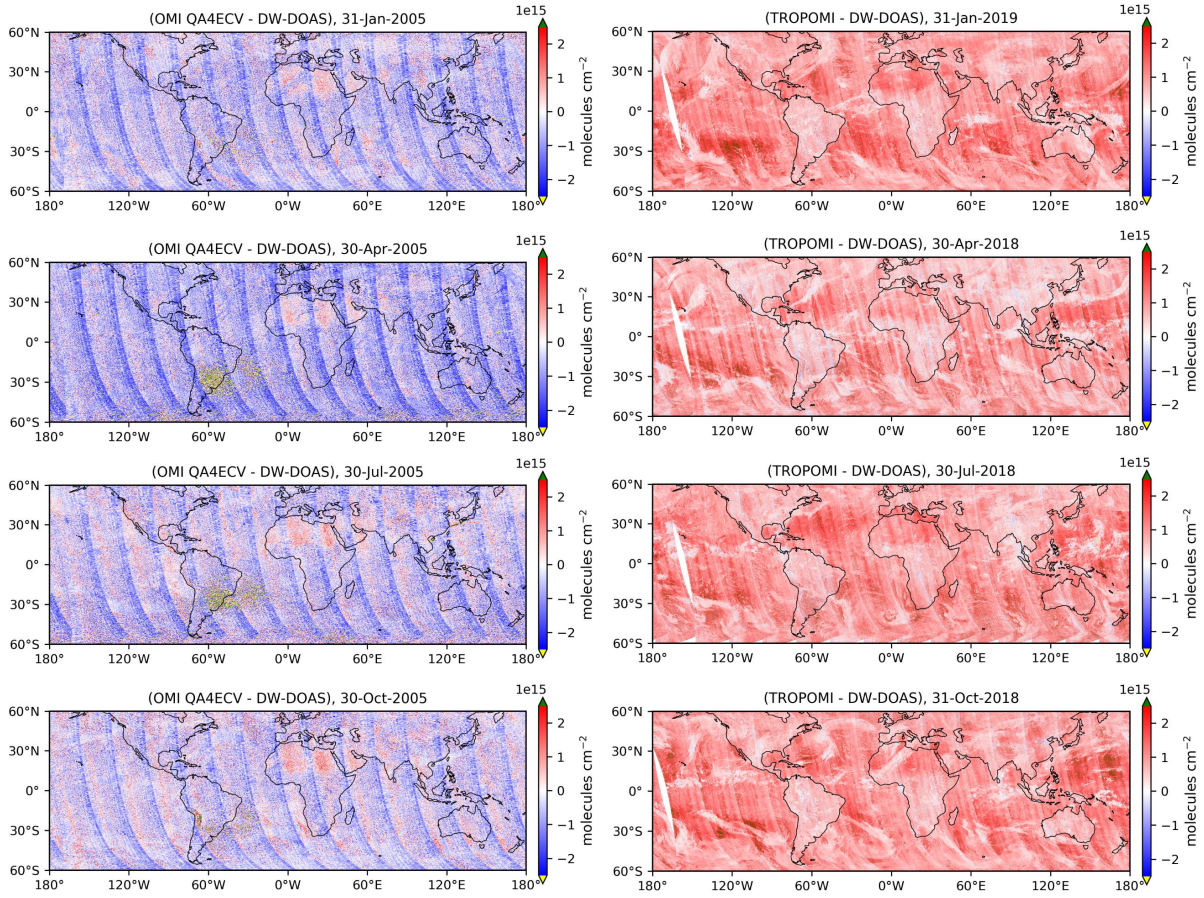

Figure A1. Absolute differences between DW-DOAS and: (left) OMI QA4ECV, and (right) TROPOMI, for the data shown in Figures 5 and 9. The differences are expressed in terms of the SCD scaled with the geometric AMF. The latitudes are limited to [60° S, 80° N].

Next steps for this work shall include optimising the DW-DOAS method, particularly the channel selection, including the selection of optimal centre wavelengths, number of channels, filter widths, and a comprehensive sensitivity study. Moreover, the practicalities of implementing this method on a real instrument need further assessment: wavelength calibration, reference spectrum (I_0) for the DOAS retrieval (Earthshine/solar spectrum), cloud retrieval, and the next stages of the NO_2 retrieval (tropospheric/stratospheric separation, and AMF calculation).

Appendix A: Absolute differences between DW-DOAS and OMI and TROPOMI

Figure A1 shows the absolute differences between the geometric column densities (i.e. SCDs scaled with the geometric AMFs) as retrieved by DW-DOAS and the OMI/TROPOMI L2 reference products.

Data availability. The OMI Level 1B data used in this work (OML1BRVG.003) are publicly available at https://disc.gsfc.nasa.gov/datasets?page=1&source=AURA%20OMI. The OMI QA4ECV NO_2 Level 2 data were obtained from http://temis.nl/airpollution/no2col/no2regioomi_qa.php. The TROPOMI Level 1B data (L1B_RA_BD4 and L1B_IR_UVN) and some of the NO_2 Level 2 data (offline products from July and October 2018, and January 2019) were obtained from https://s5phub.copernicus.eu/dhus/#/home. The TROPOMI NO_2 offline reprocessed Level 2 data from April 2018 were obtained from http://temis.nl/airpollution/no2col/no2regio_tropomi.php. The maps shown in Figures 3, 5, 7, and 9 were plotted using the cartopy Python package (Met Office, 2010 - 2015) with default coast lines, which uses freely available Natural Earth map data.

Author contributions. CRV undertook the research, prepared the figures, and wrote the manuscript. JSA, RJL, PSM, CEP and JVH provided invaluable supervision and reviewed the manuscript.

Competing interests. The authors declare that they have no conflict of interest.

Acknowledgements. This research was funded by the CENTA Doctoral Training Programme (Grant NE/L002493/1) as part of the Natural Environmental Research Council (UK), in partnership with Thales Alenia Space UK. This work follows the outcomes of the project "High-resolution Anthropogenic Pollution Imager (HAPI) on an OmniSat Platform", funded by CEOI-ST under the UKSA's NSTP Flagship programme (Grant RP10G0348C01).

~~The OMI Level 1B data used in this work (OML1BRVG.003) are publicly available at . The OMI QA4ECV NO_2 Level 2 data were obtained from . The TROPOMI Level 1B data (L1B_RA_BD4 and L1B_IR_UVN) and some of the NO_2 Level 2 data (offline products from July and October 2018, and January 2019) were obtained from . The TROPOMI NO_2 offline reprocessed Level 2 data from April 2018 were obtained from . The maps shown in Figures 3, 5, 7, and 9 were plotted using the cartopy Python package (Met Office, 2010 - 2015) with default coast lines, which uses freely available Natural Earth map data. This research used the ALICE High Performance Computing Facility at the University of Leicester.~~

We thank Jos van Geffen for kindly providing the auxiliary files (absorption cross sections) used in the OMI and TROPOMI reference products, and we are grateful to him and Folkert Boersma for advising on the analysis of the results (Tables 2 and 3).

This research used the ALICE High Performance Computing Facility at the University of Leicester.

References

Alvarado, L. M. A., Richter, A., Vrekoussis, M., Wittrock, F., Hilboll, A., Schreier, S. F., and Burrows, J. P.: An improved glyoxal retrieval from OMI measurements, Atmospheric Measurement Techniques, 7, 4133–4150, https://doi.org/10.5194/amt-7-4133-2014, https://search.proquest.com/docview/1630427902, 2014.

Anand, J. S., Monks, P. S., and Leigh, R. J.: An improved retrieval of tropospheric NO_2 from space over polluted regions using an Earth radiance reference, Atmospheric Measurement Techniques, 8, 1519–1535, https://doi.org/10.5194/amt-8-1519-2015, https://www.openaire.eu/search/publication?articleId=dedup_wf_001::0995eee3b29b32e75150a86de0cac614, 2015.

Boersma, K. F., Eskes, H. J., Veefkind, J. P., Brinksma, E. J., A, van der, R. R., Sneep, M., van den Oord GHJ, Levelt, P. P., Stammes, P., Gleason, J. F., and Bucsela, E. J.: Near-real time retrieval of tropospheric NO_2 from OMI, Atmospheric Chemistry and Physics, 7, 2103–2118, https://doi.org/10.5194/acp-7-2103-2007, https://www.narcis.nl/publication/RecordID/oai:library.tue.nl:689616, 2007.

Boersma, K. F., Eskes, H. J., Dirksen, R. J., A, van der, R. R., Veefkind, J. P., Stammes, P., Huijnen, V. V., Kleipool, Q. L., Sneep, M., Claas, J., Leitao, J., Richter, A., Zhou, Y., and Brunner, D.: An improved tropospheric NO_2 column retrieval algorithm for the ozone monitoring instrument, Atmospheric Measurement Techniques, 4, 1905–1928, https://doi.org/10.5194/amt-4-1905-2011, http://www.narcis.nl/publication/RecordID/oai:library.tue.nl:750408, 2011.

Boersma, K. F., Eskes, H., Richter, A., Smedt, I. D., Lorente, A., Beirle, S., van Geffen, J., Peters, E., Roozendael, M. V., and Wagner, T.: QA4ECV NO_2 tropospheric and stratospheric column data from OMI [Dataset], https://doi.org/10.21944/qa4ecv-NO_2-omi-v1.1, https://search.datacite.org/works/10.21944/qa4ecv-NO$_2$-omi-v1.1, 2017.

Boersma, K. F., Eskes, H. J., Richter, A., Smedt, I. D., Lorente, A., Beirle, S., van Geffen, J. H. G. M., Zara, M., Peters, E., Roozendael, M. V., Wagner, T., Maasakkers, J. D., van der A, R. J., Nightingale, J., Rudder, A. D., Irie, H., Pinardi, G., Lambert, J.-C., and Compernolle, S. C.: Improving algorithms and uncertainty estimates for satellite NO_2 retrievals: results from the quality assurance for the essential climate variables (QA4ECV) project, Atmospheric Measurement Techniques, 11, 6651–6678, https://doi.org/10.5194/amt-11-6651-2018, https://search.proquest.com/docview/2157485671, 2018.

Bovensmann, H., Burrows, J. P., Buchwitz, M., Frerick, J., Noël, S., Rozanov, V. V., Chance, K. V., and Goede, A. P. H.: SCIAMACHY: Mission Objectives and Measurement Modes, Journal of the Atmospheric Sciences, 56, 127–150, https://doi.org/SMOAMM>2.0.CO;2, https://search.proquest.com/docview/236471863, 1999.

Bucsela, E., Celarier, E., Wenig, M., Gleason, J., Veefkind, J., Boersma, K., and Brinksma, E.: Algorithm for NO_2 vertical column retrieval from the ozone monitoring instrument, IEEE Transactions on Geoscience and Remote Sensing, 44, 1245, https://doi.org/10.1109/TGRS.2005.863715, https://search.proquest.com/docview/865701973, 2006.

Burrows, J. P., Weber, M., Buchwitz, M., Rozanov, V., Ladstätter-Weißenmayer, A., Richter, A., DeBeek, R., Hoogen, R., Bramstedt, K., Eichmann, K.-U., Eisinger, M., and Perner, D.: The Global Ozone Monitoring Experiment (GOME): Mission Concept and First Scientific Results, Journal of the Atmospheric Sciences, 56, 151–175, https://doi.org/TGOMEG>2.0.CO;2, https://search.proquest.com/docview/236472213, 1999.

Castellanos, P. and Boersma, K. F.: Reductions in nitrogen oxides over Europe driven by environmental policy and economic recession, Scientific reports, 2, 265, https://doi.org/10.1038/srep00265, https://www.ncbi.nlm.nih.gov/pubmed/22355777, 2012.

Cede, A., Herman, J., Richter, A., Krotkov, N., and Burrows, J.: Measurements of nitrogen dioxide total column amounts using a Brewer double spectrophotometer in direct Sun mode, Journal of Geophysical Research - Atmospheres, 111, D05 304, https://doi.org/10.1029/2005JD006585, 2006.

Chance, K. V. and Spurr, R. J.: Ring effect studies: Rayleigh scattering, including molecular parameters for rotational Raman scattering, and the Fraunhofer spectrum, Applied optics, 36, 5224, https://doi.org/10.1364/AO.36.005224, https://www.ncbi.nlm.nih.gov/pubmed/18259337, 1997.

DEFRA: Air Pollution in the UK 2017 - Compliance Assessment Summary, Tech. rep., Department for Environment, Food & Rural Affairs, https://uk-air.defra.gov.uk/library/annualreport/assets/documents/annualreport/air_pollution_uk_2017_Compliance_Assessment_Summary_Issue1.pdf, 2018.

Dekemper, E., Vanhamel, J., Opstal, B. V., and Fussen, D.: The AOTF-based NO_2 camera, Atmospheric Measurement Techniques, 9, 6025–6034, https://doi.org/10.5194/amt-9-6025-2016, https://search.proquest.com/docview/1848748379, 2016.

Dobber, M., Kleipool, Q., Dirksen, R., Levelt, P., Jaross, G., Taylor, S., Kelly, T., Flynn, L., Leppelmeier, G., and Rozemeijer, N.: Validation of Ozone Monitoring Instrument level 1b data products, Journal of Geophysical Research - Atmospheres, 113, D15S06, https://doi.org/10.1029/2007JD008665, 2008.

Dunlea, E. J., Herndon, S. C., Nelson, D. D., Volkamer, R. M., Martini, F. S., Sheehy, P. M., Zahniser, M. S., Shorter, J. H., Wormhoudt, J. C., Lamb, B. K., Allwine, E. J., Gaffney, J. S., Marley, N. A., Grutter, M., Marquez, C., Blanco, S., Cardenas, B., Retama, A., Villegas, C. R. R., Kolb, C. E., Molina, L. T., and Molina, M. J.: Evaluation of nitrogen dioxide chemiluminescence monitors in a polluted urban environment, Atmospheric Chemistry and Physics, 7, 2691–2704, https://doi.org/10.5194/acp-7-2691-2007, https://hal.archives-ouvertes.fr/hal-00296236, 2007.

EEA: Air quality in Europe - 2018 Report, Tech. rep., European Enviroment Agency, https://www.eea.europa.eu/publications/air-quality-in-europe-2018, 2018.

EPA: Technical assistance document for the chemiluminescence measurement of nitrogen dioxide, Tech. rep., United States Environmental Protection Agency, https://www3.epa.gov/ttnamti1/archive/files/ambient/criteria/reldocs/4-75-003.pdf, ePA-600/4-75-003, 1975.

Hains, J. C., Boersma, K. F., Kroon, M., Dirksen, R. J., Cohen, R. C., Perring, A. E., Bucsela, E. J., Volten, H., Swart, D., Richter, A., Wittrock, F., Schönhardt, A., Wagner, T., Ibrahim, O. W., M, V. R., Pinardi, G., Gleason, J. F., Veefkind, J. P., and Levelt, P. P.: Testing and improving OMI DOMINO tropospheric NO_2 using observations from the DANDELIONS and INTEX-B validation campaigns, Journal of Geophysical Research. D, Atmospheres, 115, D05 301, https://doi.org/10.1029/2009JD012399, http://www.narcis.nl/publication/RecordID/oai:library.tue.nl:709618, 2010.

Heath, D. F., Krueger, A. J., Roeder, H. A., and Henderson, B. D.: The Solar Backscatter Ultraviolet and Total Ozone Mapping Spectrometer (SBUV/TOMS) for NIMBUS G, Optical Engineering, 14, https://doi.org/10.1117/12.7971839, 1975.

Hilboll, A., Richter, A., and Burrows, J. P.: NO_2 pollution over India observed from space - the impact of rapid economic growth, and a recent decline, https://doi.org/10.5194/acp-2017-101, 2017.

Huang, T., Zhu, X., Zhong, Q., Yun, X., Meng, W., Li, B., Ma, J., Zeng, E. Y., and Tao, S.: Spatial and Temporal Trends in Global Emissions of Nitrogen Oxides from 1960 to 2014, Environmental science & technology, 51, 7992–8000, https://doi.org/10.1021/acs.est.7b02235, https://www.ncbi.nlm.nih.gov/pubmed/28613845, 2017.

Ingmann, P., Veihelmann, B., Langen, J., Lamarre, D., Stark, H., and Courrèges-Lacoste, G. B.: Requirements for the GMES Atmosphere Service and ESA's implementation concept: Sentinels-4/-5 and -5p, Remote Sensing of Environment, 120, 58–69, https://doi.org/https://doi.org/10.1016/j.rse.2012.01.023, https://www.sciencedirect.com/science/article/pii/S0034425712000673, 2012.

Krijger, J. M., van Weele, M., Aben, I., and Frey, R.: Technical Note: The effect of sensor resolution on the number of cloud-free observations from space, Atmospheric Chemistry and Physics, 7, 2881–2891, https://doi.org/10.5194/acp-7-2881-2007, https://www.atmos-chem-phys.net/7/2881/2007/, 2007.

Krotkov, N. A., Lamsal, L. N., Lamsal, L. N., Celarier, E. A., Celarier, E. A., Swartz, W. H., Swartz, W. H., Marchenko, S. V., Marchenko, S. V., Bucsela, E. J., Chan, K. L., Wenig, M., and Zara, M.: The version 3 OMI NO_2 standard product, Atmospheric Measurement Techniques, 10, 3133–3149, https://doi.org/10.5194/amt-10-3133-2017, https://www.openaire.eu/search/publication?articleId=doajarticles::0c8fbe70b645b69194387759bf29ac5f, 2017.

Levelt, P. F., van den Oord, G. H. J., Dobber, M. R., Malkki, A., Visser, H., de Vries, J., Stammes, P., Lundell, J. O. V., and Saari, H.: The ozone monitoring instrument, IEEE Transactions on Geoscience and Remote Sensing, 44, 1093–1101, https://doi.org/10.1109/TGRS.2006.872333, http://ieeexplore.ieee.org/document/1624590, 2006.

Levelt, P. F., Joiner, J., Tamminen, J., Veefkind, J. P., Bhartia, P. K., Zweers, D. C. S., Duncan, B. N., Streets, D. G., Eskes, H., van der A, R., McLinden, C., Fioletov, V., Carn, S., de Laat, J., DeLand, M., Marchenko, S., McPeters, R., Ziemke, J., Fu, D., Liu, X., Pickering, K., Apituley, A., Abad, G. G., Arola, A., Boersma, F., Miller, C. C., Chance, K., de Graaf, M., Hakkarainen, J., Hassinen, S., Ialongo, I., Kleipool, Q., Krotkov, N., Li, C., Lamsal, L., Newman, P., Nowlan, C., Suleiman, R., Tilstra, L. G., Torres, O., Wang, H., and Wargan, K.: The Ozone Monitoring Instrument: overview of 14 years in space, Atmospheric Chemistry and Physics, 18, 5699–5745, https://doi.org/10.5194/acp-18-5699-2018, https://search.proquest.com/docview/2029491319, 2018.

Levy, I., Mihele, C., Lu, G., Narayan, J., and Brook, J. R.: Evaluating Multipollutant Exposure and Urban Air Quality: Pollutant Interrelationships, Neighborhood Variability, and Nitrogen Dioxide as a Proxy Pollutant, Environmental Health Perspectives, 122, 65–72, https://doi.org/10.1289/ehp.1306518, https://www.ncbi.nlm.nih.gov/pubmed/24225648, 2013.

Loyola, D. G., Gimeno García, S., Lutz, R., Argyrouli, A., Romahn, F., Spurr, R. J. D., Pedergnana, M., Doicu, A., Molina García, V., and Schüssler, O.: The operational cloud retrieval algorithms from TROPOMI on board Sentinel-5 Precursor, Atmospheric Measurement Techniques, 11, 409–427, https://doi.org/10.5194/amt-11-409-2018, https://www.atmos-meas-tech.net/11/409/2018/, 2018.

Met Office: Cartopy: a cartographic python library with a Matplotlib interface, Exeter, Devon, http://scitools.org.uk/cartopy, 2010 - 2015.

Monks, P. S., Granier, C., Fuzzi, S., Stohl, A., Williams, M. L., Akimoto, H., Amann, M., Baklanov, A., Baltensperger, U., Bey, I., Blake, N., Blake, R. S., Carslaw, K., Cooper, O. R., Dentener, F., Fowler, D., Fragkou, E., Frost, G. J., Generoso, S., Ginoux, P., Grewe, V., Guenther, A., Hansson, H. C., Henne, S., Hjorth, J., Hofzumahaus, A., Huntrieser, H., Isaksen, I. S. A., Jenkin, M. E., Kaiser, J., Kanakidou, M., Klimont, Z., Kulmala, M., Laj, P., Lawrence, M. G., Lee, J. D., Liousse, C., Maione, M., McFiggans, G., Metzger, A., Mieville, A., Moussiopoulos, N., Orlando, J. J., O'Dowd, C. D., Palmer, P. I., Parrish, D. D., Petzold, A., Platt, U., Pöschl, U., Prévôt, A. S. H., Reeves, C. E., Reimann, S., Rudich, Y., Sellegri, K., Steinbrecher, R., Simpson, D., ten Brink, H., Theloke, J., van der Werf, G. R., Vautard, R., Vestreng, V., Vlachokostas, C., and von Glasow, R.: Atmospheric composition change – global and regional air quality, Atmospheric Environment, 43, 5268–5350, https://doi.org/10.1016/j.atmosenv.2009.08.021, https://www.sciencedirect.com/science/article/pii/S1352231009007109, 2009.

Mount, G. H., Rusch, D. W., Noxon, J. F., Zawodny, J. M., and Barth, C. A.: Measurements of stratospheric NO_2 from the Solar Mesosphere Explorer satellite: 1. An overview of the results, Journal of Geophysical Research: Atmosphereres, 89, 1327–1340, http://ntrs.nasa.gov/search.jsp?R=19840040377, 1984.

Munro, R., Anderson, C., Callies, J., Corpaccioli, E., Eisinger, M., Lang, R., Lefebvre, A., Livschitz, Y., and Albiñana, A. P.: GOME-2 on MetOp, vol. 1216, p. 48, Helsinki, Finland, 2006.

Oldeman, A.: Effect of including an intensity offset in the DOAS NO2 retrieval of TROPOMI, Tech. rep., Eindhoven University of Technology/KNMI, Eindhoven, https://kfolkertboersma.files.wordpress.com/2018/06/report_oldeman_22052018.pdf, internship report, R1944-SE, 2018.

Palmer, P. I., Jacob, D. J., Chance, K., Martin, R. V., Spurr, R. J. D., Kurosu, T. P., Bey, I., Yantosca, R., Fiore, A., and Li, Q.: Air mass factor formulation for spectroscopic measurements from satellites: Application to formaldehyde retrievals from the Global Ozone Monitoring Experiment, Journal of Geophysical Research: Atmospheres, 106, 14 539–14 550, https://doi.org/10.1029/2000JD900772, https://onlinelibrary.wiley.com/doi/abs/10.1029/2000JD900772, 2001.

Platt, U. and Stutz, J.: Differential optical absorption spectroscopy: principles and applications, Springer, Berlin, ulrich Platt, Jochen Stutz.; Includes bibliographical references (p. 505 -568) and index.; Physics of earth and space environments., 2008.

Richter, A., Burrows, J. P., Nuss, H., Granier, C., and Niemeier, U.: Increase in tropospheric nitrogen dioxide over China observed from space, Nature, 437, 129–132, https://doi.org/10.1038/nature04092, http://dx.doi.org/10.1038/nature04092, 2005.

Richter, A., Begoin, M., Hilboll, A., and Burrows, J. P.: An improved NO_2 retrieval for the GOME-2 satellite instrument, Atmospheric Measurement Techniques, 4, 1147–1159, https://doi.org/10.5194/amt-4-1147-2011, https://search.proquest.com/docview/875625419, 2011.

Russell, A. R., Valin, L. C., and Cohen, R. C.: Trends in OMI NO_2 observations over the United States: effects of emission control technology and the economic recession, Atmospheric Chemistry and Physics, 12, 12 197–12 209, https://doi.org/10.5194/acp-12-12197-2012, https://search.proquest.com/docview/1266381666, 2012.

van Geffen, J., Sneep, M., Eskes, H., Boersma, K. F., ter Linden, M., and Veefkind, J. P.: S5P/TROPOMI NO2 slant column retrieval: method, stability, uncertainties, and comparisons against OMI, Atmospheric Measurement Techniques, 2019a.

van Geffen, J. H. G. M., Boersma, K. F., van Roozendael, M., Henick, F., Mahieu, E., de Smedt, I., Sneep, M., and Veefkind, J. P.: Improved spectral fitting of nitrogen dioxide from OMI in the 405–465 nm window, Atmospheric Measurement Techniques, 8, 1685–1699, https://doi.org/10.5194/amt-8-1685-2015, http://www.narcis.nl/publication/RecordID/oai:library.wur.nl:wurpubs%2F492545, 2015.

van Geffen, J. H. G. M., Eskes, H. J., Boersma, K. F., Maasakkers, J. D., and Veefkind, J. P.: TROPOMI ATBD of the total and tropospheric NO_2 data products, Tech. rep., Koninklijk Nederlands Meteorologisch Instituut (KNMI), s5PKNMIL20005RP, 2018.

van Geffen, J. H. G. M., Eskes, H. J., Boersma, K. F., Maasakkers, J. D., and Veefkind, J. P.: TROPOMI ATBD of the total and tropospheric NO_2 data products, Tech. rep., Koninklijk Nederlands Meteorologisch Instituut (KNMI), s5PKNMIL20005RP, 2019b.

Vandaele, A. C., Fayt, C., Hendrick, F., Hermans, C., Humbled, F., Roozendael, M. V., Gil, M., Navarro, M., Puentedura, O., Yela, M., Braathen, G., Stebel, K., Tørnkvist, K., Johnston, P., Kreher, K., Goutail, F., Mieville, A., Pommereau, J.-P., Khaikine, S., Richter, A., Oetjen, H., Wittrock, F., Bugarski, S., Frieß, U., Pfeilsticker, K., Sinreich, R., Wagner, T., Corlett, G., and Leigh, R.: An intercomparison campaign of ground-based UV-visible measurements of NO_2, BrO, and OClO slant columns: Methods of analysis and results for NO_2, Journal of Geophysical Research - Atmospheres, 110, D08 305, https://doi.org/10.1029/2004JD005423, https://hal.archives-ouvertes.fr/hal-00069193, 2005.

Veefkind, J. P., Aben, I., McMullan, K., Förster, H., de Vries, J., Otter, G., Claas, J., Eskes, H. J., de Haan, J. F., Kleipool, Q., van Weele, M., Hasekamp, O., Hoogeveen, R., Landgraf, J., Snel, R., Tol, P., Ingmann, P., Voors, R., Kruizinga, B., Vink, R., Visser, H., and Levelt, P. F.: TROPOMI on the ESA Sentinel-5 Precursor: A GMES mission for global observations of the atmospheric composition for climate, air quality and ozone layer applications, Remote Sensing of Environment, 120, 70–83, https://doi.org/10.1016/j.rse.2011.09.027, https://www.sciencedirect.com/science/article/pii/S0034425712000661, 2012.

Veefkind, J. P., de Haan, J. F., Sneep, M., and Levelt, P. F.: Improvements to the OMI O_2–O_2 operational cloud algorithm and comparisons with ground-based radar–lidar observations, Atmospheric Measurement Techniques, 9, 6035–6049, https://doi.org/10.5194/amt-9-6035-2016, https://www.atmos-meas-tech.net/9/6035/2016/, 2016.

Wallace, J. M. and Hobbs, P. V.: Atmospheric science, vol. 92, Elsevier Acad. Press, Amsterdam [u.a.], 2nd edn., 2006.

Wenig, M. O., Cede, A. M., Bucsela, E. J., Celarier, E. A., Boersma, K. F., Veefkind, J. P., Brinksma, E. J., Gleason, J. F., and Herman, J. R.: Validation of OMI tropospheric NO_2 column densities using direct-Sun mode Brewer measurements at NASA Goddard Space Flight Center, Journal of Geophysical Research - Atmospheres, 113, D16S45, https://doi.org/10.1029/2007JD008988, 2008.

WHO: Air quality guidelines global update 2005 : particulate matter, ozone, nitrogen dioxide, and sulfur dioxide, World Health Organization, Copenhagen, Denmark, http://ezproxy.lib.le.ac.uk/login?url=http://site.ebrary.com/lib/leicester/Doc?id=10190678, includes bibliographical references.; Ebrary eBook, 2006.

WHO Regional Office for Europe: Review of evidence on health aspects of air pollution – REVIHAAP Project, Tech. rep., WHO Regional Office for Europe, http://www.euro.who.int/__data/assets/pdf_file/0004/193108/REVIHAAP-Final-technical-report.pdf, 2013.

WMO: World Meteorological Organization: Systematic Observation Requirements for Satellite-Based Data Products for Climate – 2011 Update, Tech. rep., World Meteorological Organization, https://library.wmo.int/doc_num.php?explnum_id=3710, 2011.

Zara, M., Boersma, K. F., Smedt, I. D., Richter, A., Peters, E., van Geffen, J. H. G. M., Beirle, S., Wagner, T., Roozendael, M. V., Marchenko, S., Lamsal, L. N., and Eskes, H. J.: Improved slant column density retrieval of nitrogen dioxide and formaldehyde for OMI and GOME-2A from QA4ECV: intercomparison, uncertainty characterisation, and trends, Atmospheric Measurement Techniques, 11, 4033–4058, https://doi.org/10.5194/amt-11-4033-2018, https://search.proquest.com/docview/2067743488, 2018.